

## Research Article

# Geological and Geochemical Characteristics of the First Member of the Cretaceous Qingshankou Formation in the Qijia Sag, Northern Songliao Basin, Northeast China: Implication for Its Shale Oil Enrichment

Fei Xiao <sup>1,2</sup>, Jianguo Yang <sup>1</sup>, Shichao Li,<sup>1</sup> Fanhao Gong,<sup>1</sup> Jian Zhang,<sup>1</sup> Yulai Yao,<sup>1</sup> Ang Li,<sup>1</sup> Liyan Zhang,<sup>1</sup> Yiming Huang,<sup>1</sup> Fei Su,<sup>1</sup> and Yunfeng Bai<sup>3</sup>

<sup>1</sup>Shenyang Center of China Geological Survey, Shenyang 110034, China

<sup>2</sup>State Key Laboratory of Organic Geochemistry (SKLOG), Guangzhou Institute of Geochemistry, Chinese Academy of Sciences, Guangzhou 510640, China

<sup>3</sup>Exploration and Development Research Institute of Daqing Oilfield Co Ltd., Daqing 163712, China

Correspondence should be addressed to Jianguo Yang; yangjianguo@mail.cgs.gov.cn

Received 3 April 2021; Accepted 26 June 2021; Published 16 August 2021

Academic Editor: Guohui Chen

Copyright © 2021 Fei Xiao et al. This is an open access article distributed under the Creative Commons Attribution License, which permits unrestricted use, distribution, and reproduction in any medium, provided the original work is properly cited.

The Qijia Sag, a secondary tectonic unit in the northern Songliao Basin, developed plentiful shale oil resources in the first member of the Cretaceous Qingshankou Formation ( $K_2qn_1$ ) as its main target layer. However, the systematic study on the geological and geochemical characteristics of  $K_2qn_1$  in the sag has not been carried out. Taking the core samples from the SYY1 well covering the whole  $K_2qn_1$  as the main study object and concerning some relevant intervals from the SYY1HF well and other earlier wells, petrologic features, organic geochemical characteristics, oil-bearing property, and reservoir characteristics of  $K_2qn_1$  were analyzed in detail. The results show that the lithology of  $K_2qn_1$  is mainly dark mudstone genera accounting for more than 90% of the formation thickness with few macrostructural fractures, indicating that  $K_2qn_1$  developing in deep to semideep lacustrine facies of the Qijia Sag belongs to the typical matrix reservoirs for shale oil. According to lithology features and logging curves,  $K_2qn_1$  can be divided into three submembers consisting of  $K_2qn_1^1$ ,  $K_2qn_1^2$ , and  $K_2qn_1^3$  from above to below. Compared to the  $K_2qn_1^1$  submember, the  $K_2qn_1^2$  and  $K_2qn_1^3$  submembers obviously are more enriched in shale oil, which is supported by the following three aspects: (i) the average TOC (total organic carbon) values of  $K_2qn_1^1$ ,  $K_2qn_1^2$ , and  $K_2qn_1^3$  are 1.96%, 2.42%, and 2.72%, respectively. The organic matter types of  $K_2qn_1^2$  and  $K_2qn_1^3$  are mainly type I and type II<sub>1</sub>, while those of  $K_2qn_1^1$  are mainly type II<sub>1</sub> and type II<sub>2</sub>.  $K_2qn_1$  is at the end of the oil window with a  $R_o$  (vitrinite reflectance) average of 1.26%, and the maturity of  $K_2qn_1^2$  and  $K_2qn_1^3$  is slightly higher than that of  $K_2qn_1^1$ . (ii) The average OSI (oil saturation index) values of  $K_2qn_1^1$ ,  $K_2qn_1^2$ , and  $K_2qn_1^3$  are 110.54 mg/g, 171.74 mg/g, and 150.87 mg/g, respectively, which all reach the zone of oil crossover. The saturated hydrocarbon of EOM (extractable organic matter) in  $K_2qn_1^2$  and  $K_2qn_1^3$  is of higher content than that in  $K_2qn_1^1$ , while it is the opposite for the aromatic hydrocarbon, nonhydrocarbon, and asphaltene, indicating better oil mobility for  $K_2qn_1^2$  and  $K_2qn_1^3$ . The average oil saturation values of  $K_2qn_1^1$ ,  $K_2qn_1^2$ , and  $K_2qn_1^3$  are 24.77%, 32.86%, and 35.54%, respectively. (iii) The intragranular dissolution pores and organic pores in  $K_2qn_1^2$  and  $K_2qn_1^3$  are more developed than those in  $K_2qn_1^1$ . The average effective porosity values of  $K_2qn_1^1$ ,  $K_2qn_1^2$ , and  $K_2qn_1^3$  interpreted from NMR logging are 4.88%, 6.26%, and 5.86%, respectively. Based on the above-mentioned analyses, the lower  $K_2qn_1^2$  and the upper  $K_2qn_1^3$  are determined as the best intervals of shale oil enrichment for  $K_2qn_1$  vertically in the Qijia Sag. There is a certain horizontal heterogeneity of TOC,  $S_1$ , and effective porosity in the drilling horizontal section of  $K_2qn_1$  of the SYY1HF well. Therefore, the lower  $K_2qn_1^2$  and the upper  $K_2qn_1^3$  in the area with relatively weak horizontal reservoir heterogeneity of the study area should be selected as the preferential targets for shale oil exploration.

## 1. Introduction

As the commercial development of shale oil was achieved in North America, shale oil/reservoir has been one of the hottest fields for petroleum exploration and geological study. Shale oil is defined as the generated and unexpelled residual petroleum occurring in organic-rich shale strata series with three occurrence states of free, adsorbed, and dissolved oils, in which the free oil is the main potential recoverable part under the widely used exploitation technology of hydraulic fracturing [1, 2]. According to the report from EIA (U.S. Energy Information Administration), Russia, U.S., and China occupy the top three of the technically recoverable shale oil resources in the world [3]. Through the shale revolution, U.S. took the lead in successively achieving the commercial development of shale gas and shale oil, which has attracted great attention from many petroleum companies and explorers of other countries. China began to carry out shale gas exploration works since 2005 [4], and the commercial development of marine shale gas in the southern China was realized in 2015 [5]. However, the exploration of shale oil, especially for the oil reserved in the nano-micron pores and microfractures of the shale matrix rather than in nonshale interlayers and macrofractures, is still in the initial stage. Unlike shale oils in the U.S., which mainly occur in marine shale strata series, shale oils in China are mainly distributed in the lacustrine shale strata series of the petroliferous basins such as Songliao, Bohai Bay, Ordos, Sichuan, Juggar, and Jiangnan [6–12]. Due to different characteristics of water environment, sediment sources, biotic input, and buried history from the marine shale strata series in the U.S., the lacustrine shale strata series in China are generally characterized by stronger lithofacies heterogeneity and lower maturity [4, 6, 12–15], which makes reservoir fracturing and shale oil extraction more challenging.

The Songliao Basin is a large lacustrine basin in the northeast China (Figure 1(a)) with 11.5 billion barrels of technically recoverable shale oil [3]. The Upper Cretaceous Qingshankou Formation ( $K_2qn$ ), the main hydrocarbon generation strata in the Songliao Basin, is also the main target of shale oil exploration [16–19]. The  $K_2qn$  can be divided into two members, the first member in the lower ( $K_2qn_1$ ) and the second-third member in the upper ( $K_2qn_{2+3}$ ) (Figure 2). The northern Songliao Basin belongs to the main exploration area of the Daqing Oilfield, and its shale oil exploration of the Qingshankou Formation has roughly experienced three stages. During the first stage, the exploration of shale oil accumulating in mudstone fractured reservoirs started in 1981, aimed at the lower  $K_2qn_{2+3}$  and the upper  $K_2qn_1$  in the Gulong Sag, and industrial oil flows were approached in the Y12, Y18, H16, and GP1 wells [18, 19]. As the significant continuous shale oil productions were not realized in the above wells, i.e., the low yield and rapid oil yield decay, the relative exploration works were slowed down. During the second stage, the exploration of shale oil in sandstone interbedded reservoirs started in 2011, aimed at the delta outer front facies of the lower  $K_2qn_{2+3}$  in the Qijia Sag, and high production industrial oil flows were discovered in several horizontal wells including the QP1 and QP1-1 wells [20,

21]. The resource of desert areas for this kind of shale oil was estimated to be  $1.5 \times 10^8$  t in the Qijia Sag [22]. Recently for the third stage, the exploration of shale oil in the  $K_2qn_1$  shale reservoirs started in 2016. Cooperating with the Daqing Oilfield, the China Geological Survey deployed and implemented several shale oil parameter wells, including the SYY1 and SYY1HF wells in the Qijia Sag and the SYY2 and SYY2HF wells in the Gulong Sag. Industrial oil flows were achieved in the SYY1 and SYY2 wells, and high production industrial oil flows were achieved in the SYY1HF and SYY2HF wells. Good results have been approached through the producing tests of the SYY1HF and SYY2HF wells, which indicates huge resource potential for shale oil in the  $K_2qn_1$  shale reservoirs [23]. The  $K_2qn_1$  in the Qijia and Gulong sags was regarded as the most promising exploration field of shale oil in the northern Songliao Basin [24, 25].

The previous geological and geochemical studies of shale oil in the northern Songliao Basin were focused on the Gulong Sag [6, 26–30], less involving in the Qijia Sag. Moreover, all these studies were based on the incomplete core data, which cannot represent the detailed profile characteristics of  $K_2qn_1$ . A full-section coring of  $K_2qn_1$  was performed on the SYY-1 well, which lays a good foundation for the further detailed study in the Qijia Sag. Therefore, the SYY1 well as the main object combining other well data including the newly drilled SYY1HF well in the study area created very good conditions for this study. This paper is aimed at comprehensively analyzing the geological and geochemical characteristics of  $K_2qn_1$  in detail through the analytical test, mud logging, and logging data and thus determining the shale oil enrichment regularity of  $K_2qn_1$  in the Qijia Sag.

## 2. Geological Setting

The Songliao Basin located in the northeastern China (Figure 1(a)) is a Mesozoic-Cenozoic continental petroliferous basin superimposing on the Hercynian fold basement. It is about 750 km long and 350 km wide with an area of  $2.6 \times 10^5$  km<sup>2</sup> [31], and the long axis direction of the basin is northeast-southwest (Figure 1(b)). According to the development characteristics of strata and faults during the depression period, the Songliao Basin can be divided into six first-order structural units, including the Central Depression, the Northern Plunge, the Northeastern Uplift, the Southeastern Uplift, the Southwestern Uplift, and the Western Slope [16]. Taking the central line of the basin as a boundary, the exploration area to the north of the boundary (the northern Songliao Basin) mainly belongs to the Daqing Oilfield of PetroChina, while the exploration area to the south of the boundary (the southern Songliao Basin) mainly belongs to the Jilin Oilfield of PetroChina and the Northeast Petroleum Bureau of Sinopec (Figure 1(b)). The Qijia Sag as the study area of this paper is one of the second-order structural units of the Central Depression, adjacent to the north of the Gulong Sag (Figure 1(c)). The area of the Qijia Sag is about 2225 km<sup>2</sup>.

According to the regional tectonic setting, tectonic style, sedimentary evolution, volcanic activity, and thermal history, the formation and development of the Songliao Basin

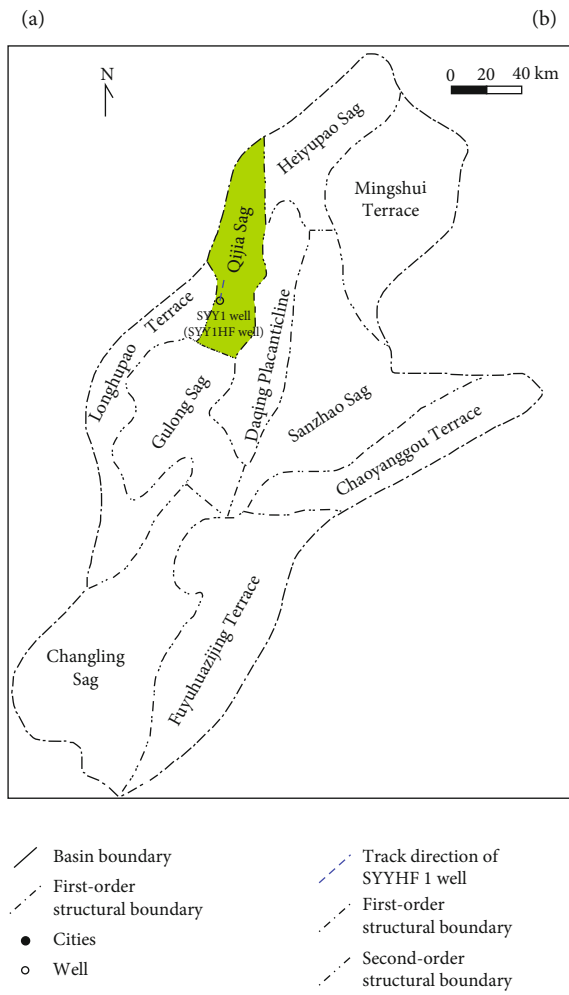
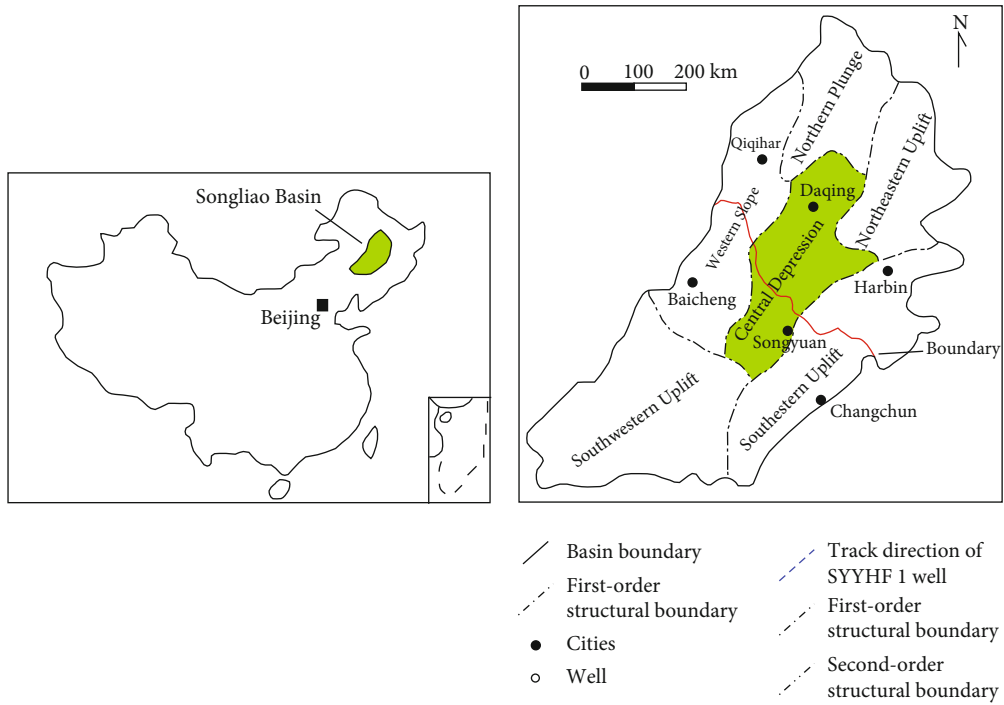


FIGURE 1: Location of the study area and structural unit division of the Songliao Basin (modified from [16]).

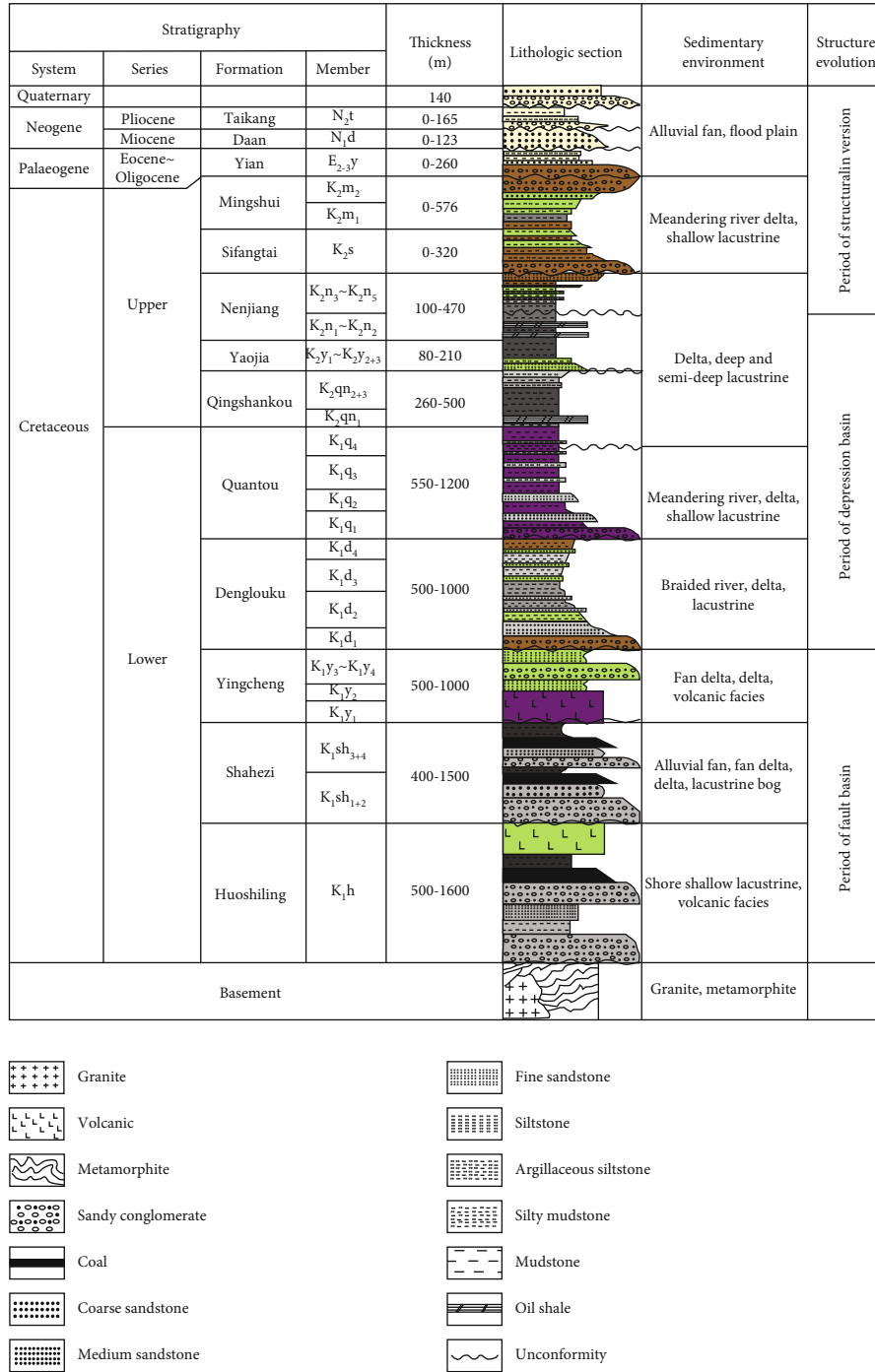


FIGURE 2: Comprehensive stratigraphic column of the Songliao Basin.

experienced three evolution periods of fault basin, depression basin, and structural inversion (Figure 2) since the Cretaceous [31–33]. The Cretaceous strata, the main hydrocarbon-bearing series developed in the basin, consist of the Lower Cretaceous Huoshiling, Shahezi, Yingcheng, Denglouku, and Quantou formations and the Upper Cretaceous Qingshankou, Yaojia, Nenjiang, Sifangtai, and Mingshui formations from below to above (Figure 2). The oil and gas in the Songliao Basin are mainly distributed in the Daqing Placanticline, the Qijia Sag, the Gulong Sag, the

Sanzhao Sag, and the Changling Sag of the Central Depression (Figure 1(c)).

The SYY1 well located in the southern Qijia Sag is a vertical parametric well for shale oil exploration, and the SYY1HF well is the horizontal well adjusted from the SYY1 well with an azimuth of 10.97 degrees (Figure 1(c)). It must be pointed out that vertical well hydraulic fracturing was conducted on the K<sub>2</sub>qn<sub>1</sub> and the bottom of K<sub>2</sub>qn<sub>2+3</sub> of the SYY1 well before the drilling of the SYY1HF well.

### 3. Data and Methods

**3.1. Petrographic Description.** Coring operation was conducted on the whole  $K_2qn_1$  section of the SYY1 well in the Qijia Sag at the depth from 2357.00 m to 2448.00 m, and the characteristics of lithology, fossils, and sedimentary structure of the cores were described in detail with a scale of 1 : 10. Meanwhile, a few pictures of typical geological phenomena of cores were taken and collected. Based on that, the vertical petrographic distribution of  $K_2qn_1$  in the Qijia Sag can be analyzed. Because there was no coring in the SYY1HF well, the lithologic description data of  $K_2qn_1$  rock debris collected from the mud logging were adopted to study the horizontal lithology distribution of  $K_2qn_1$ .

#### 3.2. Mineral and Reservoir Analyses

**3.2.1. X-Ray Diffraction Mineral Analysis.** A total of 21 core samples from  $K_2qn_1$  of the SYY1 well were analyzed by means of the German Brook D8A A25 X-ray Diffractive Instrument in order to obtain the percentage composition of whole rock minerals and clay minerals. For the SYY1HF well, the percentage composition data of whole rock minerals of 214  $K_2qn_1$  core debris samples were collected from the X-ray diffraction mud logging.

**3.2.2. Effective Porosity Analysis.** The effective porosity of 15 core samples from  $K_2qn_1$  of the SYY1 well was conducted on the PoroPDP-200 Instrument from the American Core Lab Company. In order to solve the problem of a small number of measured data, the high-resolution effective porosity data of the SYY1 and SYY1HF wells were obtained through the nuclear magnetic resonance (NMR) logging interpretation calibrated by the measured data.

**3.2.3. NMR Laboratory Analysis.** A total of 37 core samples from  $K_2qn_1$  of the SYY1 well were analyzed at room temperature by means of the MR Core-XX NMR Analyzer from the American Core Lab Company in order to obtain the oil saturation data.

**3.2.4. Argon Ion Polishing-Scanning Electron Microscopy.** Considering lithology and depth distribution, 14 core samples were selected from  $K_2qn_1$  of the SYY1 well. The samples were cut into suitable blocks (10 mm × 10 mm × 3 mm), and the block samples were manually polished using the sandpapers with various degree of roughness. Then, the samples were polished for 6 hours at 4 kV voltage with high-energy argon ion beam on the Ilion<sup>+</sup>II 697C Polisher from the American Gatan Company. Finally, the microscopic pore structures of the samples were observed on the Quanta 450 Scanning Electron Microscopy from the American FEI Company.

#### 3.3. Organic Geochemical Analyses

**3.3.1. Total Organic Carbon (TOC) and Rock Pyrolysis.** A total of 81 core samples from the  $K_2qn_1$  of the SYY1 well were selected according to the lithofacies. TOC and rock pyrolysis tests of those samples were performed on the American LECO CS Analyzer and French VINCI Rock-Eval 6 Ana-

lyzer, respectively. The commonly used geochemical parameters including pyrolysed hydrocarbon ( $S_1$ ), kerogen pyrolytic hydrocarbon ( $S_2$ ), and maximum pyrolysis peak temperature ( $T_{max}$ ) were approached by rock pyrolysis.

**3.3.2. Microscopic Examination of Kerogen.** The microscopic observation of kerogen macerals of 7 core samples from  $K_2qn_1$  of the SYY1 well was conducted on the German Leica-DM45009 Microscope. Before the microscopic observation, the samples were made into polished sections according to petroleum and natural gas industry standard of the People's Republic of China (SY/T 6414-2014). The composition of kerogen macerals including sapropelite, exinite, vitrinite, and inertinite was counted and recorded.

**3.3.3. Vitrinite Reflectance ( $R_o$ ).** The reflectance of vitrinite of 5 core samples from the  $K_2qn_1$  of the SYY1 well was tested using oil-immersed objective lens by means of the German Leica DM4500P Polarizing Microscope and American CRAIC Microphotometer. Before the microscopic observation, the samples were made into polished sections according to the petroleum and natural gas industry standard of the People's Republic of China (SY/T 5124-2012). In order to ensure the testing accuracy of the results, the number of measuring points should not be less than 30 for each sample.

**3.3.4. Extraction and Column Chromatography of Soluble Organic Matter.** A total of 21 core samples from the  $K_2qn_1$  of the SYY1 well were selected, and Soxhlet extraction and column chromatographic separation were performed on these samples. First, the samples were crushed into 100 mesh and extracted for 24 h with dichloromethane, and the content of extractable organic matter (EOM) was confirmed. Then, asphaltenes in the EOM were removed and measured by n-hexane precipitation. After that, the deasphalted EOM were separated by silica gel and alumina column chromatography, and saturated and aromatic hydrocarbon fractions were obtained by the flushing of the n-hexane and the mixture of n-hexane and dichloromethane (volume ratio 2 : 1), respectively. Finally, nonhydrocarbon was obtained by the flushing of chloroform.

## 4. Results and Discussion

### 4.1. Petrologic Features and Submember Division

**4.1.1. Petrologic Features.** The lithology of  $K_2qn_1$  in the SYY1 well consists of mainly gray-black/black mudstone, gray/gray-black silty mudstone, and black Ostracoda-bearing mudstone, locally interbedded with gray-black argillaceous siltstone, gray siltstone, and gray/gray-black Ostracoda layers (Figure 3, Table 1). In addition, black-gray marl and gray-white tuffite can be found sporadically. Pyrite aggregates, carbonaceous fragments, plant fossil fragments, Ostracoda, Eosetheria fossils, and horizontal beddings were generally observed throughout the cores (Figure 3, Table 1). From the geological mud logging data, the lithology of  $K_2qn_1$  in the SYY1HF well consists of black-gray silty mudstone and gray-black mudstone. The all above evidences suggest that  $K_2qn_1$  was deposited in the deep and semideep lacustrine

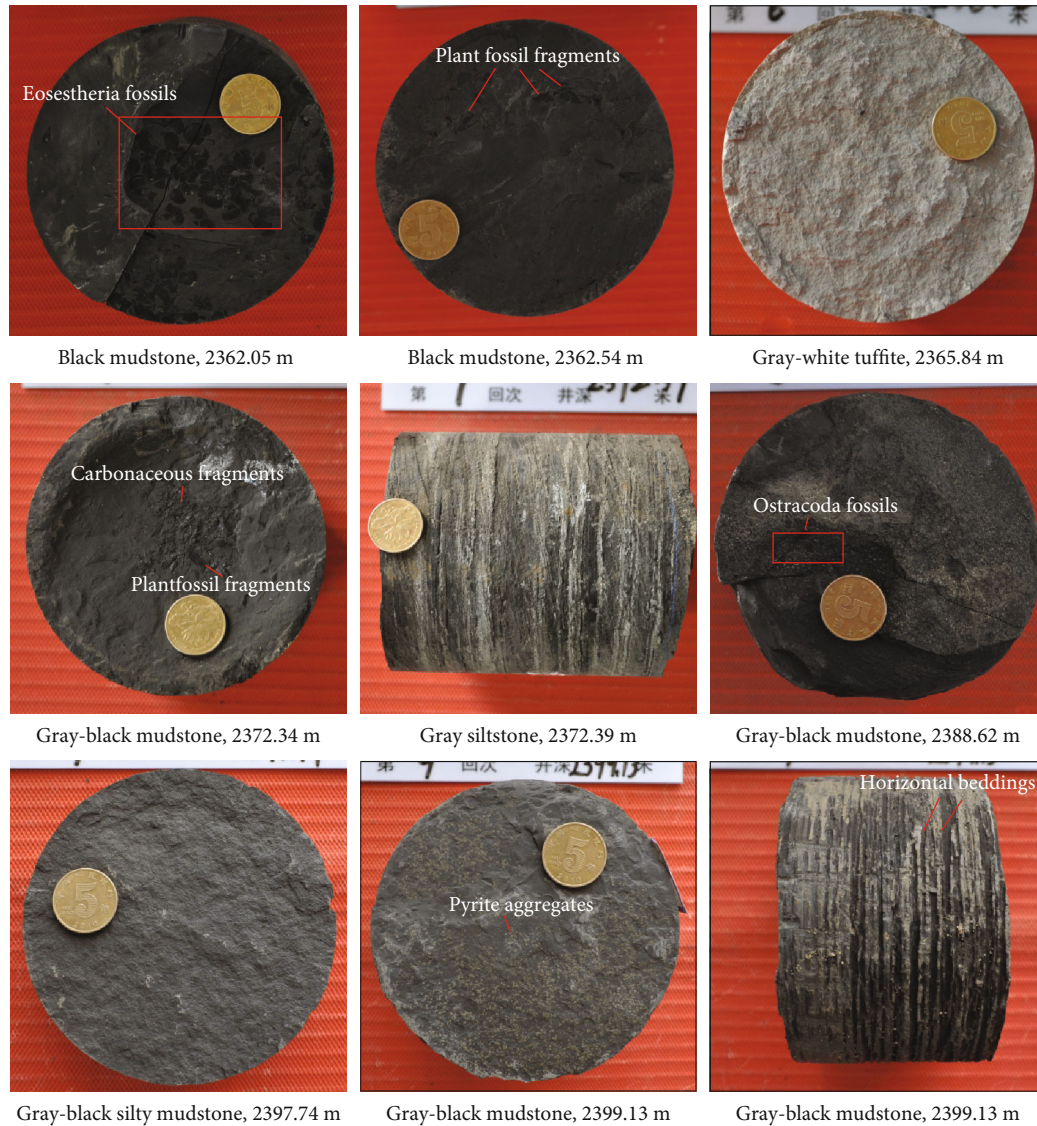


FIGURE 3: Pictures of typical lithology and sedimentary structure of the  $K_2qn_1$  cores in the SYY1 well, Qijia Sag, northern Songliao Basin.

environment with volcanic activities around the lacustrine water. The thickness of mudstone genera is 86.12 m, accounting for 94.64% of the  $K_2qn_1$  thickness in the SYY1 well (Table 1), and the macrostructural fractures were not developed in the cores, indicating that  $K_2qn_1$  belongs to the typical matrix reservoirs for shale oil. Thus, the reservoir spaces of  $K_2qn_1$  may be mainly matrix pores and microfractures of mudstones.

Minerals in  $K_2qn_1$  of the SYY1 well are mainly composed of clay minerals, quartz, and plagioclase, containing a small amount of calcite and pyrite with dolomite, K-feldspar, ankerite, and siderite in some parts (Figure 4). The content of clay minerals ranges from 7.80% to 45.20% (36.37% on average), while the content of quartz and plagioclase ranges from 27.20% to 42.0% (35.20% on average) and from 7.50% to 50.80% (18.50% on average), respectively. It indicates that siliceous minerals are the dominant component in  $K_2qn_1$  core samples. The content of calcite ranges from 0.70% to 27.10% (5.85% on average). The high abundances of carbon-

ate minerals at the depths of 2378.83 m and 2402.67 m (Figure 4) are related to ostracod biodeposition. Based on the mineral compositions, Allix and Burnham divided the shale/mudstone into five types including siliceous mudstone, argillaceous mudstone (traditional shale), siliceous marlstone, argillaceous marlstone, and calcareous or dolomitic mudstone [34]. From Figure 5, most of the  $K_2qn_1$  samples of SYY1 and SYY1HF wells are mainly siliceous mudstones, and a few are argillaceous mudstones, which are similar to the Lower Marcellus and Bakken shales in North America (Figure 5).

**4.1.2. Submember Division of  $K_2qn_1$ .** Based on the lithology features and logging curves, the connected well profile of  $K_2qn_1$  crossing the X81, SYY1, X91, and X83 wells in the Qijia Sag was drawn, and  $K_2qn_1$  in the study area can be divided into three submembers including  $K_2qn_1^1$ ,  $K_2qn_1^2$ , and  $K_2qn_1^3$  from above to below (Figure 6). The  $K_2qn_1^1$  submember is characterized by developing nonmudstone thin

TABLE 1: Lithology statistical summary table of  $K_2qn_1$  cores in the SYY1 well, Qijia Sag, northern Songliao Basin.

Genera	Color	Lithology	Thickness (m)		Percentage (%)	
			Single value	Subtotal value	Single value	Subtotal value
Mudstone	Gray-black/black	Mudstone	73.50		80.77	
	Gray/gray-black	Silty mudstone	7.93		8.72	
	Black	Ostracoda-bearing mudstone	3.97	86.12	4.36	94.64
	Black/gray-black	Ostracoda-bearing silty mudstone	0.64		0.70	
	Gray-black	Calcareous mudstone	0.08		0.09	
Siltstone	Gray-black	Argillaceous siltstone	1.65		1.81	
	Gray	Siltstone	1.63		1.79	
	Black-gray	Calcareous siltstone	0.60	4.21	0.66	4.63
	Gray-black	Ostracoda-bearing siltstone	0.18		0.19	
	Gray	Ostracoda-bearing siltstone	0.15		0.17	
Ostracoda layer	Gray/gray-black	Ostracoda layer		0.54		0.60
Marlstone	Black-gray	Marlstone		0.08		0.09
Tuffite	Gray-white	Tuffite		0.05		0.05
Total value	/	/		91.00		100.00

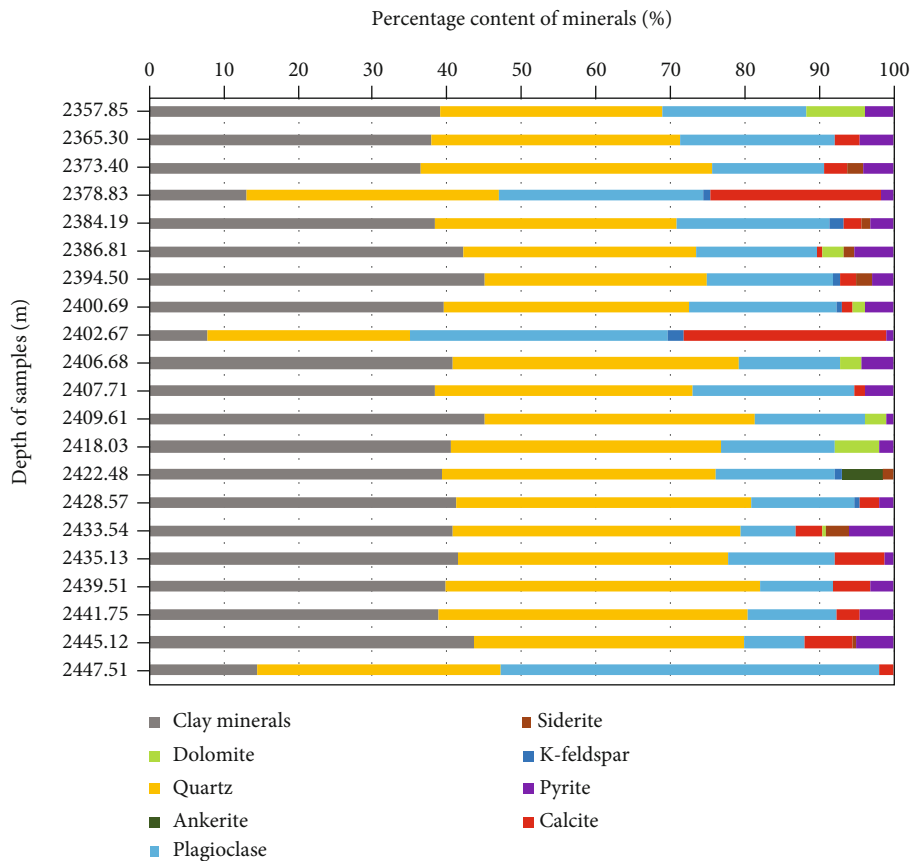


FIGURE 4: Diagram of mineral composition of the  $K_2qn_1$  core samples in the SYY1 well, Qijia Sag, northern Songliao Basin.

intercalations in the whole submember, low-medium natural gamma, and low-medium resistivity, corresponding to the depth from 2357.00 m to 2390.00 m in the SYY1 well. The  $K_2qn_1^2$  submember is characterized by developing nonmud-

stone thin intercalations mainly in the middle-upper submember, medium natural gamma, and medium-high resistivity, corresponding to the depth from 2390.00 m to 2418.50 m in the SYY1 well. The  $K_2qn_1^3$  submember is

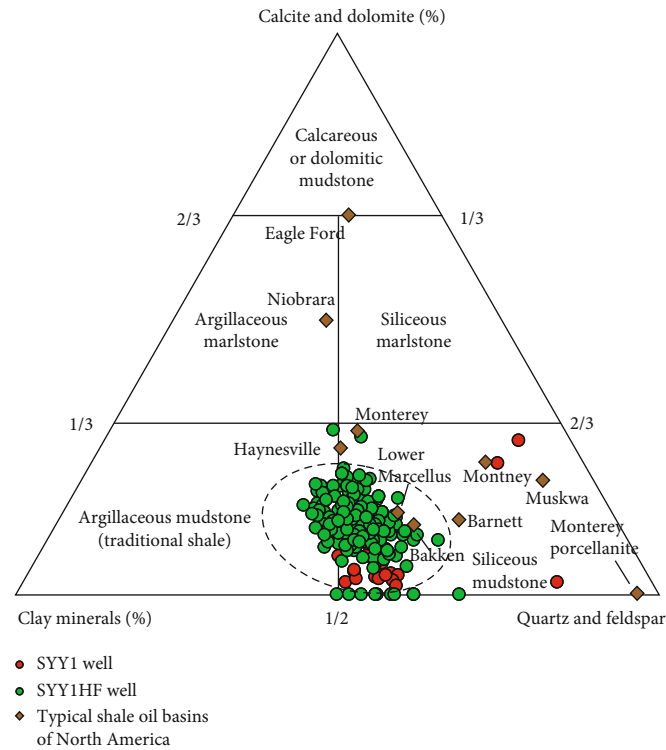


FIGURE 5: Ternary diagram showing the mineral compositions of the  $K_2qn_1$  samples in the SYY1 and SYY1HF wells and the samples from some typical shale oil basins of North America (sample data of the typical shale oil basins of North America are from Reference [34]).

characterized by developing nonmudstone thin intercalations mainly in the middle-lower submember, high natural gamma, and medium-high resistivity, corresponding to the depth from 2418.50 m to 2448.00 m in the SYY1 well. The target layer of the SYY1HF well corresponds to the upper  $K_2qn_1^3$  submember at the depth from 2419 m to 2429 m in the SYY1 well (Figure 6).

#### 4.2. Organic Geochemical Characteristics

**4.2.1. Organic Matter Abundance.** Total organic carbon (TOC) and  $S_1 + S_2$  are two commonly used parameters for the evaluation of organic matter abundance in shale/mudstone [35–37]. Both the parameters show that the organic matter abundance of  $K_2qn_1$  in the SYY1 well is generally high, and most of the TOC and  $S_1 + S_2$  values are greater than 2.0% and 6.0 mg/g, respectively. Both the two parameters increase first and then decrease with the increase in buried depth (Figure 7). From the perspective of three submembers, the TOC values of  $K_2qn_1^1$ ,  $K_2qn_1^2$ , and  $K_2qn_1^3$  range from 1.30% to 2.68% (1.96% on average), from 0.87% to 3.73% (2.42% on average), and from 1.12% to 5.04% (2.72% on average), respectively (Figure 7(a)), and the  $S_1 + S_2$  values of  $K_2qn_1^1$ ,  $K_2qn_1^2$ , and  $K_2qn_1^3$  range from 3.27 mg/g to 10.02 mg/g (6.39 mg/g on average), from 4.86 mg/g to 23.77 mg/g (13.03 mg/g on average), and from 3.96 mg/g to 25.33 mg/g (13.06 mg/g on average), respectively (Figure 7(b)). It indicates that  $K_2qn_1^2$  and  $K_2qn_1^3$  are of higher organic matter abundance than  $K_2qn_1^1$ , and the lower  $K_2qn_1^2$  and the upper  $K_2qn_1^3$  have the highest organic matter

abundance (Figure 7). Shale oil is characterized by in situ retention and enrichment [38], so the high organic matter abundance in the lower  $K_2qn_1^2$  and the upper  $K_2qn_1^3$  created a very good hydrocarbon-generating material base for their shale oil enrichment.

From the TOC variation characteristics of well logging interpretation of  $K_2qn_1$  in the SYY1HF well, the overall trend of TOC value increasing from top boundary depth of  $K_2qn_1$  to the depth of target A (drilling inclined section of  $K_2qn_1$ ) can be observed (Figures 8(a) and 8(b)), which is consistent with the results from the SYY1 well (Figure 7(a)). The TOC values at the drilling inclined section of  $K_2qn_1$  in the SYY1HF well range from 0.64% to 4.09% with an average of 2.06%, while the TOC values at the drilling horizontal section of  $K_2qn_1$  range from 0.62% to 5.69% with an average of 2.45% (Figures 8(a) and 8(b)). Furthermore, the TOC values at the drilling horizontal section fluctuated greatly, and the TOC values near target A are distinctly higher than those near target C (Figures 8(a) and 8(b)), which indicates that the abundance of organic matter in  $K_2qn_1$  is highly heterogeneous horizontally.

**4.2.2. Organic Matter Type.** Whether shale as source rock is oil-prone or gas-prone mainly depends on organic matter types, which are generally classified into four categories including type I, type II<sub>1</sub>, type II<sub>2</sub>, and type III. Among them, the type I and type II<sub>1</sub> kerogens are oil-prone with high hydrocarbon generation potential, while the type II<sub>2</sub> and type III kerogens are gas-prone with low hydrocarbon generation potential [39, 40]. The  $HI-T_{max}$  discriminant chart and the



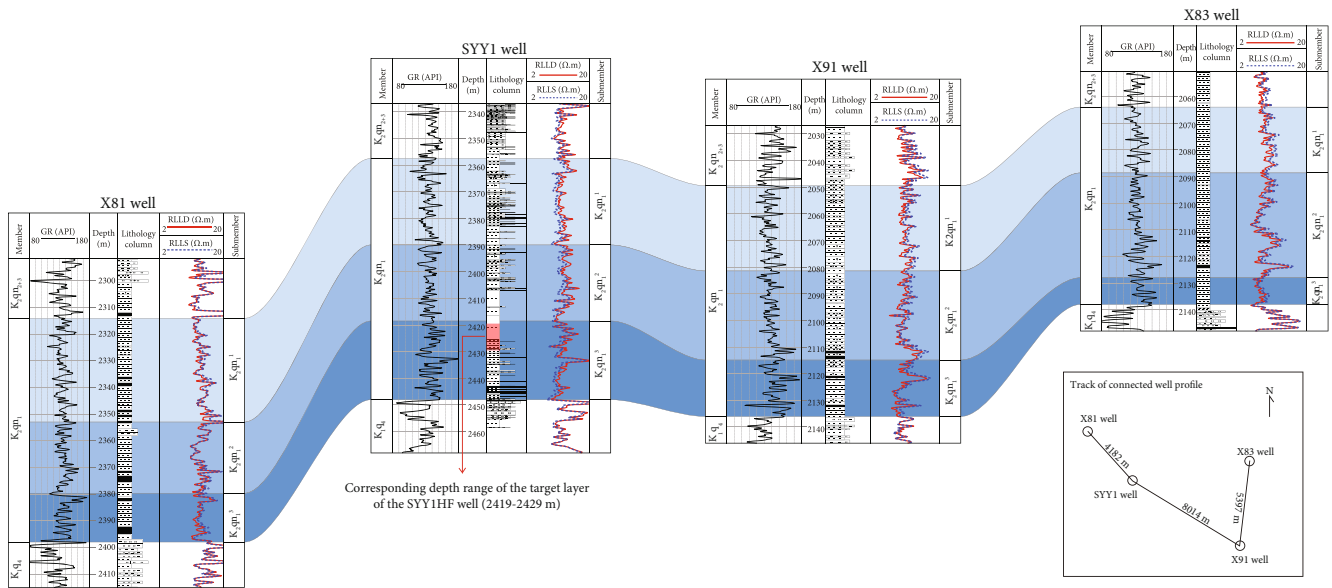


FIGURE 6: Connected well profile of  $K_2qn_1$  crossing the X81, SYY1, X91, and X83 wells in the Qijia Sag, northern Songliao Basin.

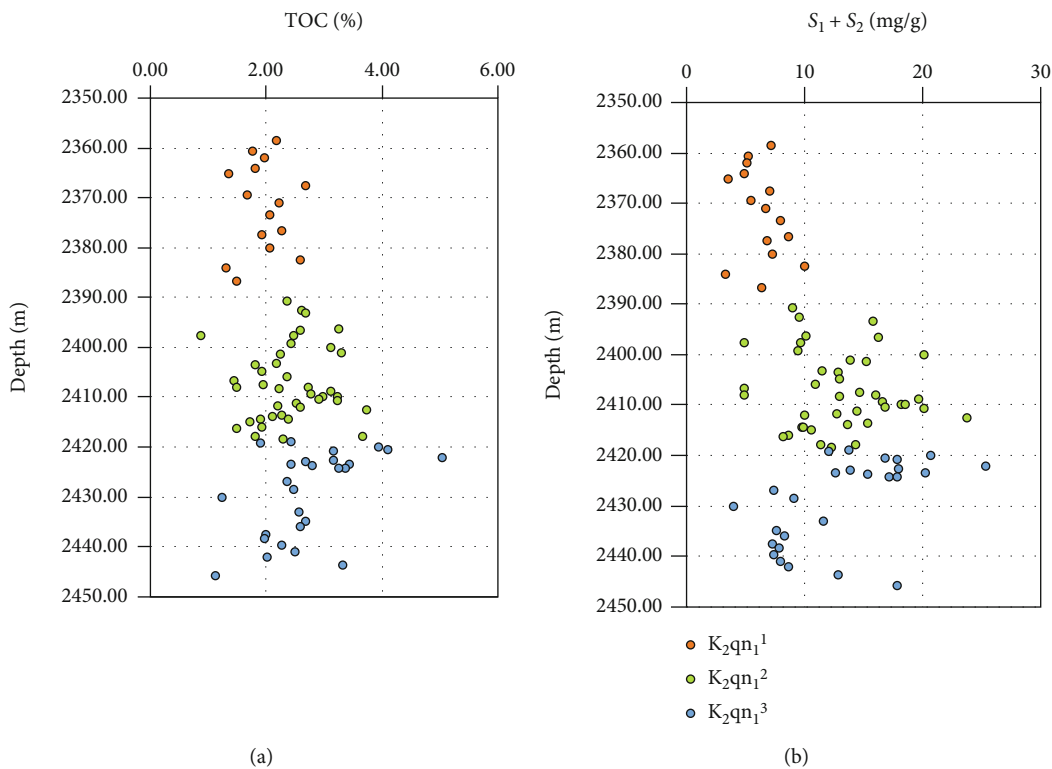


FIGURE 7: Graphs of TOC (a) and  $S_1 + S_2$  (b) variation with the depth of  $K_2qn_1$  core samples in the SYY1 well, Qijia Sag, northern Songliao Basin.

kerogen maceral analysis are two commonly used methods for determining organic matter types. The  $HI-T_{max}$  discriminant chart shows that the organic matter types of the  $K_2qn_1$  core samples in the SYY1 well are mainly type I and type  $II_1$  with a small number of type  $II_2$  (Figure 9), indicating the oil-prone feature for  $K_2qn_1$  organic matter. The  $K_2qn_1$  kerogen maceral groups from the SYY1 well are mostly oil-prone

sapropelite, followed by gas-prone inertinite and vitrinite with little exinite (Figure 10), which also proves that  $K_2qn_1$  is oil-prone generally. However,  $K_2qn_1^2$  and  $K_2qn_1^3$  have better organic matter types than  $K_2qn_1^1$ . The organic matter types of  $K_2qn_1^2$  and  $K_2qn_1^3$  submembers are mainly type I and type  $II_1$  with a small number of type  $II_2$ , while those of the  $K_2qn_1^1$  submember are mainly type  $II_1$  and type  $II_2$

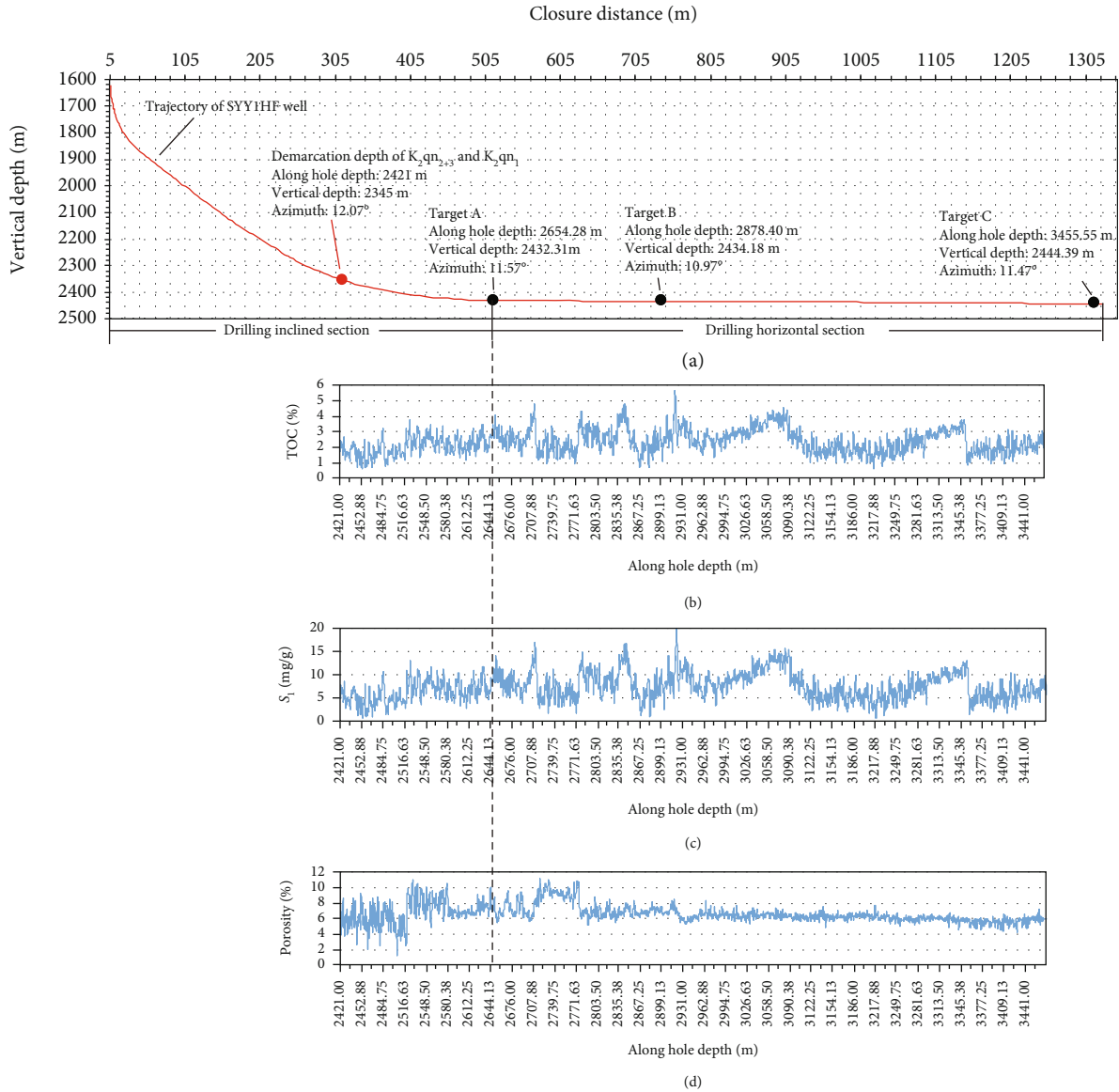


FIGURE 8: Trajectory diagram of the SYY1HF well (a) and distribution diagrams of well logging interpretation TOC (b),  $S_1$  (c), and effective porosity (d) in the drilling horizontal section of the SYY1HF well, Qijia Sag, northern Songliao Basin.

without type I (Figure 9), indicating better oil generation potential for the  $K_2qn_1^2$  and  $K_2qn_1^3$  submembers.

**4.2.3. Organic Matter Maturity.** The maturity of organic matter reflects the degree of transformation from organic matter to oil and gas, and the products of organic matter are varied in different stages of thermal evolution [35, 37, 39]. Therefore, the amount of retained oil in shale and its mobility are closely related to the maturity of organic matter, and only the shale oil with medium-high maturity can be effectively exploited by hydraulic fracturing technology at present [4].  $R_o$  and  $T_{max}$  are two commonly used parameters to evaluate the maturity of organic matter. However, relevant studies have shown that  $T_{max}$  is greatly affected by organic matter types and is more suitable for the maturity assessment of gas-prone organic matter of type III and type  $II_2$  [39, 41]. As mentioned above, the organic matter types of the studied

samples are mainly oil-prone type I and type  $II_2$ , so  $R_o$  is adopted here to evaluate the sample maturity. The measured  $R_o$  values of five  $K_2qn_1$  samples in the SYY1 well range from 1.21% to 1.28% with an average of 1.26% (Table 2), indicating that those samples are at the end of the oil window. Such high maturity indicates that crude oil has been produced in large quantities and, if not expelled, can remain and accumulate in shale/mudstone. In addition, shale oil at this stage of thermal evolution can be of better fluidity and better recoverability because of having more light components. The  $R_o$  values increase slightly with the increase in depth (Table 2), indicating that the maturity of the lower part of  $K_2qn_1$  is slightly higher than that of the upper part of that. From the plane, deep to semideep lacustrine facies in the Qijia Sag is usually located in the central sag with large burial depth, so the maturity is generally high, which can create a good thermal evolution condition for shale oil enrichment.

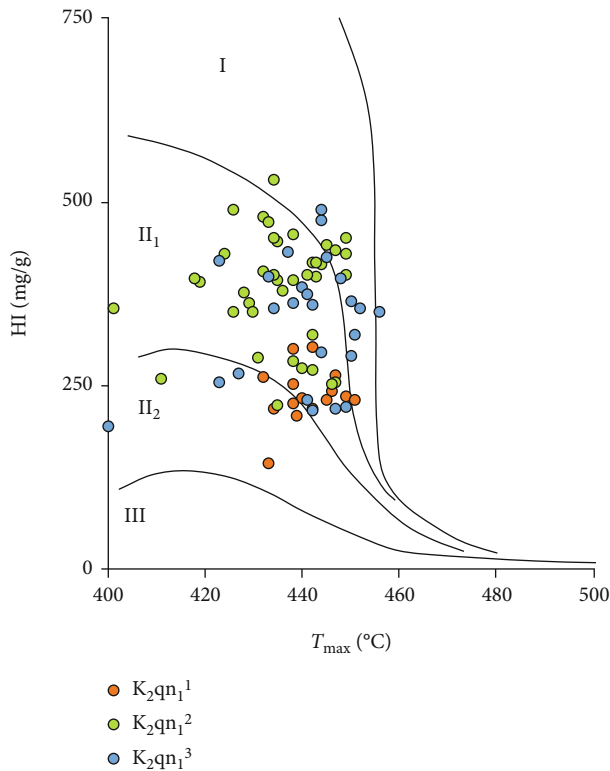


FIGURE 9: HI- $T_{max}$  discriminant chart showing the organic matter types of  $K_2qn_1$  core samples in the SY1 well, Qijia Sag, northern Songliao Basin.

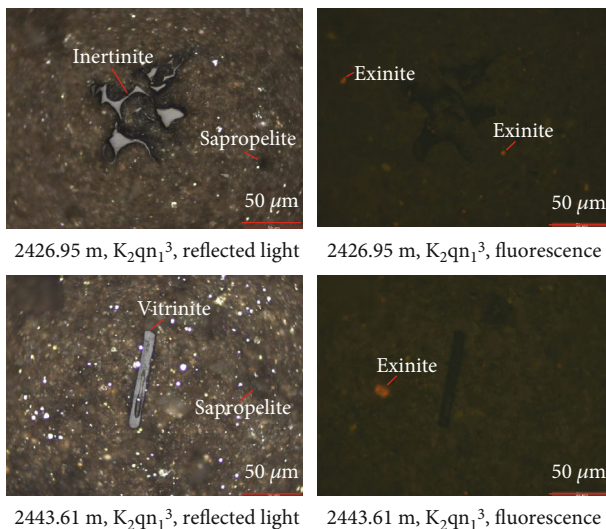


FIGURE 10: Kerogen maceral pictures of the typical  $K_2qn_1$  core samples in the SY1 well, Qijia Sag, northern Songliao Basin.

### 4.3. Oil-Bearing Property

**4.3.1. Pyrolysis  $S_1$  and OSI.** Pyrolysis  $S_1$  represents that relatively light liquid hydrocarbons exist in rocks before heating to 300°C in the Rock-Eval analysis and is used as a common oil-bearing parameter to characterize the content of free hydrocarbon in shales [42, 43]. The  $S_1$  values of  $K_2qn_1^1$ ,

$K_2qn_1^2$ , and  $K_2qn_1^3$  in the SY1 well range from 1.32 mg/g to 2.91 mg/g (2.16 mg/g on average), from 1.65 mg/g to 7.25 mg/g (4.11 mg/g on average), and from 1.93 mg/g to 7.71 mg/g (4.25 mg/g on average), respectively (Figure 11(a)). It indicates that  $K_2qn_1^2$  and  $K_2qn_1^3$  are of higher oil content than  $K_2qn_1^1$ . Furthermore, the lower  $K_2qn_1^2$  and the upper  $K_2qn_1^3$  obviously have the best oil content (Figure 11(a)). The  $S_1$  values from well logging interpretation at the drilling horizontal section of the SY1HF well fluctuated greatly, and the  $S_1$  values near target A are distinctly greater than those near target C (Figures 8(a) and 8(c)), which indicates that the oil-bearing content of  $K_2qn_1$  is highly heterogeneous horizontally.

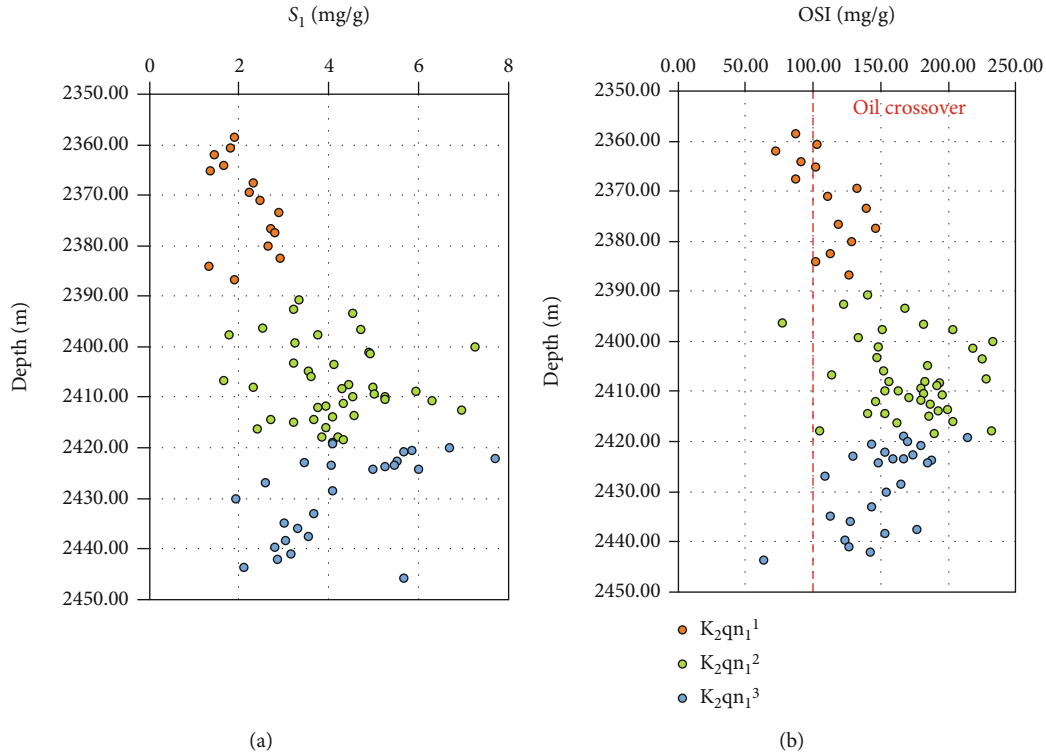
According to the results of Jarvie’s study [42], there is a certain threshold for free oil flowing in shale, and the OSI parameter (oil saturation index,  $S_1 \times 100/TOC$ ) is required to exceed 100 mg/g, which is considered the oil crossover effect. The OSI values for most of the  $K_2qn_1$  samples in the SY1 well are greater than 100 mg/g (Figure 11(b)), indicating that  $K_2qn_1$  generally is of high oil content with good oil mobility. From the perspective of three submembers, the OSI values of  $K_2qn_1^1$ ,  $K_2qn_1^2$ , and  $K_2qn_1^3$  in the SY1 well range from 72.73 mg/g to 145.83 mg/g (110.54 mg/g on average), from 77.61 mg/g to 233.16 mg/g (171.74 mg/g on average), and from 63.25 mg/g to 213.76 mg/g (150.87 mg/g on average), respectively (Figure 11(b)). It indicates that  $K_2qn_1^3$  can have more producible oils than  $K_2qn_1^1$  and  $K_2qn_1^2$ , and the lower  $K_2qn_1^2$  and the upper  $K_2qn_1^3$  obviously have the highest oil content with the best oil mobility.

**4.3.2. EOM and Group Composition.** EOM (extractable organic matter), the products extracted from shale by chloroform or other organic solvents, is another common oil-bearing parameter. Compared with pyrolysis  $S_1$ , EOM is more similar to shale oil composition, containing not only light hydrocarbons (saturated and aromatic hydrocarbons) of pyrolysis  $S_1$  but also heavy hydrocarbons, nonhydrocarbon, and asphaltene [43]. The content of EOM in the SY1 well increases firstly and then decreases with the increase in depth (Figure 12(a)). The EOM contents of  $K_2qn_1^1$ ,  $K_2qn_1^2$ , and  $K_2qn_1^3$  in the SY1 well range from 0.47% to 1.02% (0.66% on average), from 0.82% to 1.47% (1.16% on average), and from 0.39% to 1.56% (0.98% on average), respectively (Figure 12(a)). That indicates that  $K_2qn_1^2$  and  $K_2qn_1^3$  are of higher oil content than  $K_2qn_1^1$ , and the lower  $K_2qn_1^2$  and the upper  $K_2qn_1^3$  obviously have the highest oil content.

From the group compositions of EOM of  $K_2qn_1$  samples in the SY1 well, the contents of saturated hydrocarbon are the highest, followed by those of nonhydrocarbon and aromatic hydrocarbon, and those of asphaltene are the lowest (Figures 12(b)–12(e)). The average contents of saturated hydrocarbon, nonhydrocarbon, aromatic hydrocarbon, and asphaltene are 83.62%, 7.82%, 5.94%, and 2.62%, respectively (Figures 12(b)–12(e)). Compared with the other group compositions, saturated hydrocarbon molecules are smaller in volume and polarity, so the overall mobility of  $K_2qn_1$  shale oil is good, which is conducive to the oil production. With the depth increasing, the contents of saturated hydrocarbon increased, while the contents of aromatic hydrocarbon,

TABLE 2: Measurement data table of vitrinite reflectance ( $R_o$ ) of  $K_2qn_1$  cores in the SY1 well, Qijia Sag, northern Songliao Basin.

Depth (m)	Submember	Total number of measuring points	Maximum reflectivity (%)	Minimum reflectivity (%)	Mean reflectivity (%)	Mean value (%)
2358.48	$K_1qn_1^1$	34	1.34	1.06	1.21	
2382.50	$K_1qn_1^1$	30	1.35	1.17	1.28	
2396.23	$K_1qn_1^2$	35	1.35	1.08	1.25	1.26
2409.91	$K_1qn_1^2$	32	1.35	1.13	1.26	
2438.25	$K_1qn_1^3$	31	1.35	1.11	1.28	

FIGURE 11: Graphs of  $S_1$  (a) and OSI (b) variation with the depth of  $K_2qn_1$  core samples in the SY1 well, Qijia Sag, northern Songliao Basin.

nonhydrocarbon, and asphaltene decreased (Figures 12(b)–12(e)), so the lower part of  $K_2qn_1$  has better shale oil mobility than the upper part of that. In particular for  $K_2qn_1^3$ , the contents of saturated hydrocarbon are the highest of the three submembers, while the contents of aromatic hydrocarbon, nonhydrocarbon, and asphaltene are all the lowest. That can be related to the maximum burial depth and the highest maturity of the  $K_2qn_1^3$  submember. Therefore, there are more small molecules with lower polar in the composition of shale oil of the  $K_2qn_1^3$  submember, which has better oil mobility.

**4.3.3. Oil Saturation.** Oil saturation reflects the volume proportion occupied by oil in the reservoir space and directly represents the content of potentially recoverable free oil and dissolved oil in the shale. The oil saturations of  $K_2qn_1$  samples in the SY1 well range from 12.54% to 54.32% with an average of 32.78% (Figure 13). Among the three submembers, the oil saturations of  $K_2qn_1^1$  range from 12.54% to

39.83% (24.77% on average); the oil saturations of  $K_2qn_1^2$  range from 13.77% to 54.32% (32.86% on average); the oil saturations of  $K_2qn_1^3$  range from 26.86% to 42.53% (35.54% on average) (Figure 13). On the whole,  $K_2qn_1^2$  and  $K_2qn_1^3$  have higher oil saturation and better oil content.

#### 4.4. Reservoir Characteristics

**4.4.1. Reservoir Space.** The reservoir space of  $K_2qn_1$  samples in the SY1 well mainly consists of intergranular micropores and microfractures, intercrystal micropores and microfractures, and intragranular dissolution pores, with organic pores found locally (Figure 14). The composition of clastic grains is mainly quartz and feldspar, and clay minerals are mostly filled between grains in the form of squama shape. The spherical pyrite crystals are developed in the form of star-shaped, patchy, or band-like distribution (Figures 14(a), 14(i), and 14(o)), and the crystals of calcite and rutile can be seen (Figures 14(e), 14(g), 14(i), and 14(n)). The intergranular

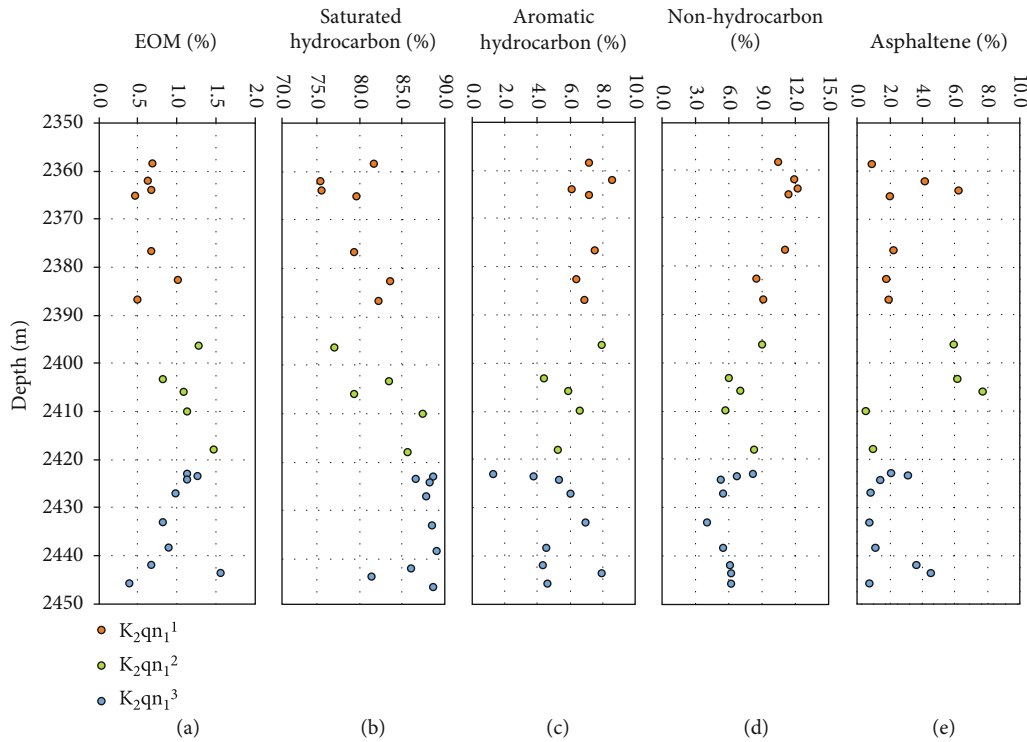


FIGURE 12: Graphs of EOM (a), saturated hydrocarbon (b), aromatic hydrocarbon (c), nonhydrocarbon (d), and asphaltene (e) variation with the depth of  $K_2qn_1$  core samples in the SY1 well, Qijia Sag, northern Songliao Basin.

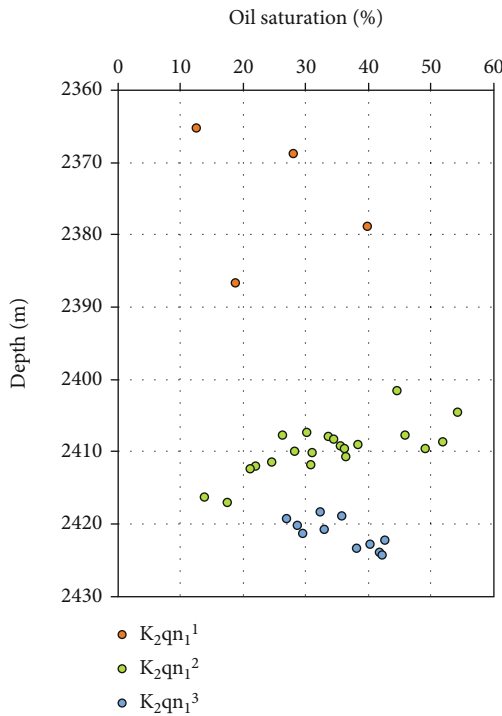


FIGURE 13: Graph of oil saturation with the depth of  $K_2qn_1$  core samples in the SY1 well, Qijia Sag, northern Songliao Basin.

micropores and microfractures consist of the primary intergranular micropores and microfractures and the clastic grain edge microfractures. The intercrystal micropores and micro-

fractures consist of intercrystalline micropores and microfractures of clay minerals (Figures 14(d) and 14(o)), intercrystalline pores of pyrites (Figures 14(a) and 14(o)), cleavage cracks of mineral crystals (Figures 14(i) and 14(m)), and intercrystalline microfractures. The intragranular dissolution pores are distributed mainly in the clastic grains of quartz and feldspar (Figures 14(b), 14(h), and 14(l)), followed by calcite grains (Figures 14(g) and 14(i)), and also developed in mineral crystals such as rutiles (Figures 14(e) and 14(n)).

Interestingly, it seems that the intragranular dissolution pores in the lower part are more developed than those in the upper part, which is reflected in the number of dissolution pores increasing and the pore size becoming bigger gradually from above to below (Figure 14). Coincidentally, it shows a similar trend for the distribution characteristics of organic pores. In the  $K_2qn_1^1$  submember and the upper  $K_2qn_1^2$  submember, the organic pores are hard to be found (Figures 14(c) and 14(f)). However, in the lower  $K_2qn_1^2$  submember and the  $K_2qn_1^3$  submember, the organic pores are much developed. They are distributed in clusters, and the pore size can reach hundreds of nanometers (Figures 14(j), 14(k), and 14(p)). The related studies show that the development degree of organic pores increases with the increase in maturity, and organic pores develop in a large number only when  $R_o$  exceeds a certain critical value [44, 45]. Therefore, maturity is one of the important reasons for the difference in the development of organic pores of  $K_2qn_1$ . According to the distribution characteristics and the sample maturities as mentioned above, we infer that there may be a maturity

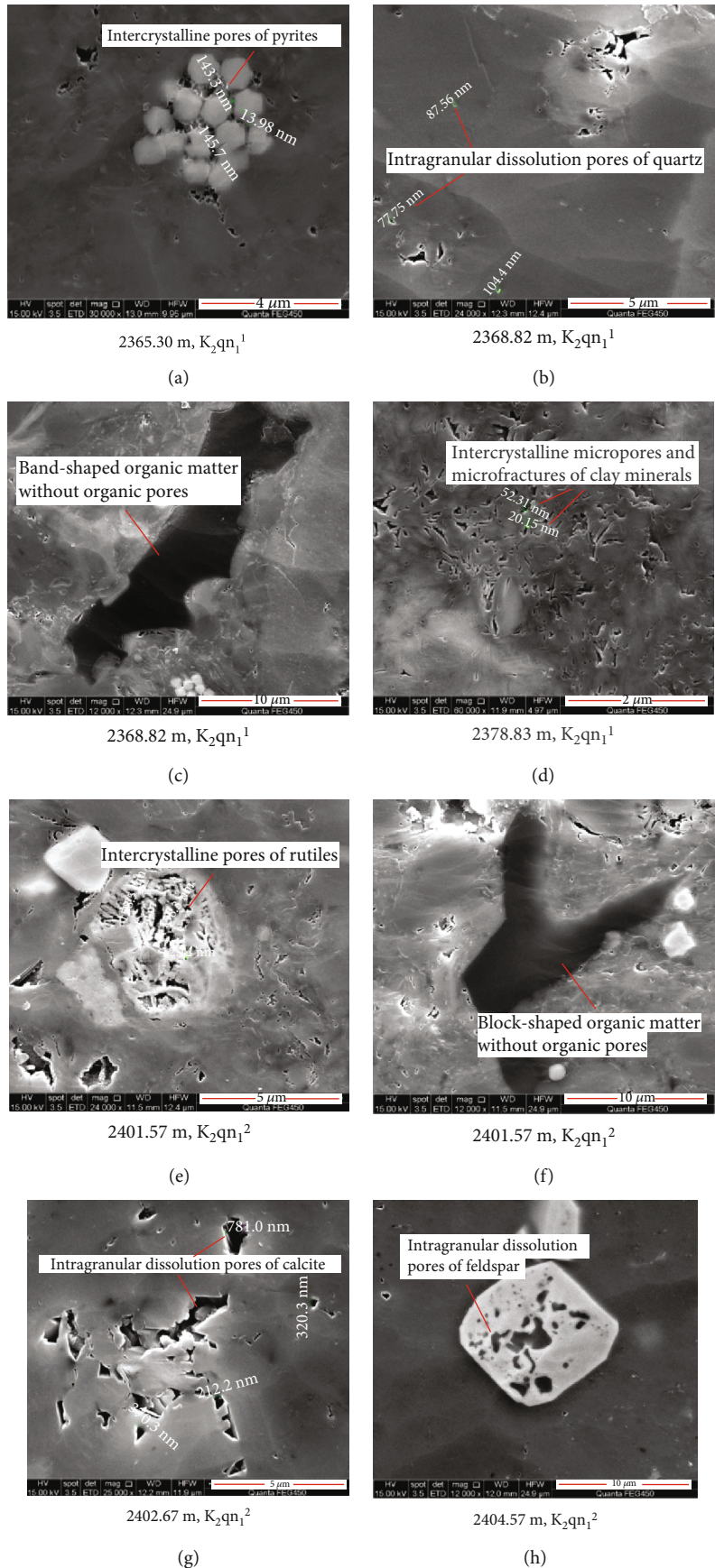


FIGURE 14: Continued.

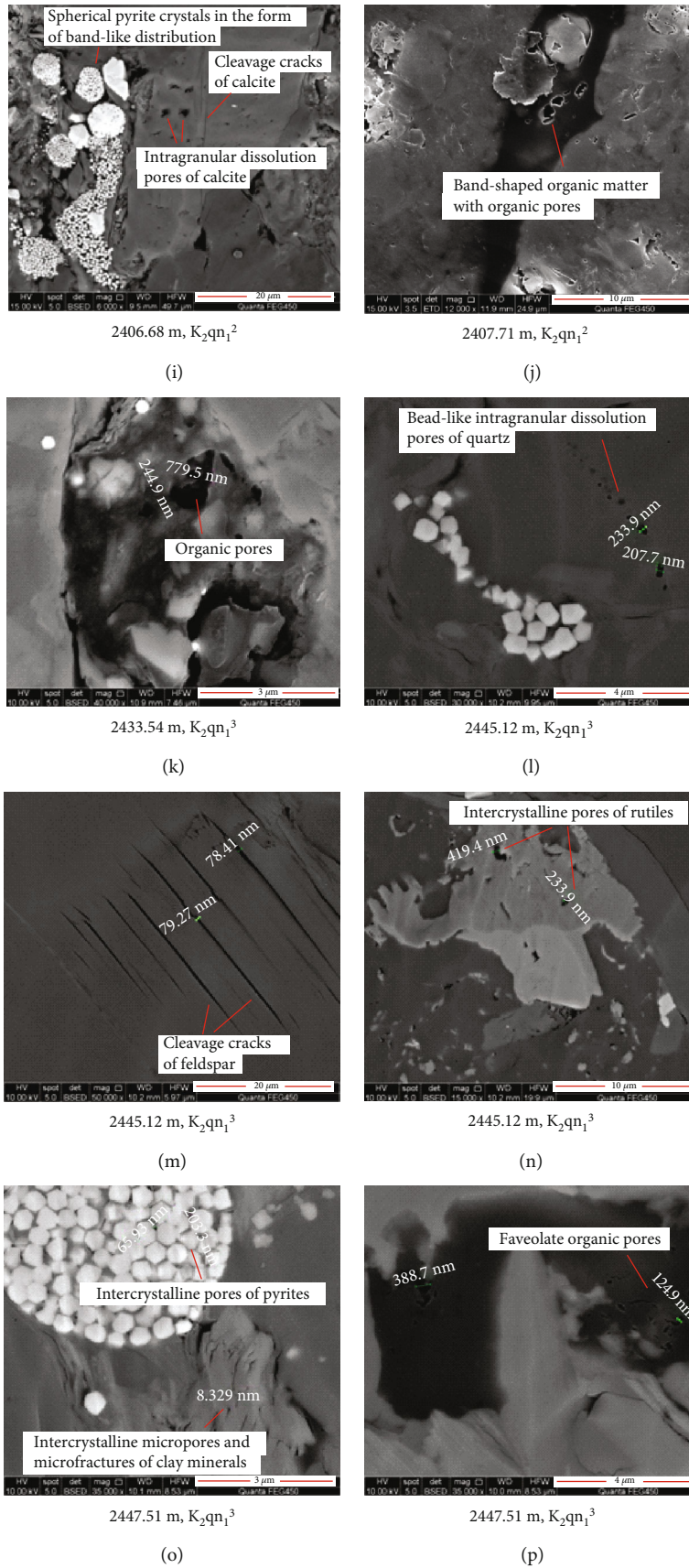


FIGURE 14: Argon ion polishing-scanning electron microscopy pictures showing the typical reservoir space of the  $K_2qn_1$  core samples in the SYY1 well, Qijia Sag, northern Songliao Basin.

TABLE 3: Percentage content data table of clay minerals of K<sub>2</sub>qn<sub>1</sub> cores in the SYY1 well, Qijia Sag, northern Songliao Basin.

Depth (m)	Submembers	Percentage content of clay minerals (%)				Composition of I/S (%)	
		Illite	Chlorite	Illite/smectite mixed layer mineral (I/S)	Chlorite/smectite mixed layer mineral (C/S)	Smectite in I/S	Illite in I/S
2357.85	K <sub>2</sub> qn <sub>1</sub> <sup>1</sup>	40	9	49	2	15	85
2365.30	K <sub>2</sub> qn <sub>1</sub> <sup>1</sup>	33	31	15	21	25	75
2373.40	K <sub>2</sub> qn <sub>1</sub> <sup>1</sup>	87	6	7	/	15	85
2378.83	K <sub>2</sub> qn <sub>1</sub> <sup>1</sup>	41	20	36	3	15	85
2384.19	K <sub>2</sub> qn <sub>1</sub> <sup>1</sup>	78	10	12	/	15	85
2386.81	K <sub>2</sub> qn <sub>1</sub> <sup>1</sup>	88	4	8	/	15	85
2394.50	K <sub>2</sub> qn <sub>1</sub> <sup>2</sup>	89	5	6	/	15	85
2400.69	K <sub>2</sub> qn <sub>1</sub> <sup>2</sup>	83	5	8	4	15	85
2402.67	K <sub>2</sub> qn <sub>1</sub> <sup>2</sup>	56	25	9	10	15	85
2406.68	K <sub>2</sub> qn <sub>1</sub> <sup>2</sup>	74	13	13	/	15	85
2407.71	K <sub>2</sub> qn <sub>1</sub> <sup>2</sup>	54	8	37	1	15	85
2409.61	K <sub>2</sub> qn <sub>1</sub> <sup>2</sup>	41	8	48	3	15	85
2418.03	K <sub>2</sub> qn <sub>1</sub> <sup>2</sup>	83	10	7	/	20	80
2422.48	K <sub>2</sub> qn <sub>1</sub> <sup>3</sup>	65	14	21	/	15	85
2428.57	K <sub>2</sub> qn <sub>1</sub> <sup>3</sup>	78	10	12	/	15	85
2433.54	K <sub>2</sub> qn <sub>1</sub> <sup>3</sup>	74	10	14	2	15	85
2435.13	K <sub>2</sub> qn <sub>1</sub> <sup>3</sup>	73	16	11	/	25	75
2439.51	K <sub>2</sub> qn <sub>1</sub> <sup>3</sup>	76	13	11	/	15	85
2441.75	K <sub>2</sub> qn <sub>1</sub> <sup>3</sup>	43	13	40	4	15	85
2445.12	K <sub>2</sub> qn <sub>1</sub> <sup>3</sup>	72	12	11	5	15	85
2447.51	K <sub>2</sub> qn <sub>1</sub> <sup>3</sup>	64	22	14	/	15	85



Diagenetic stages		Organic matter			Mudstone		Degree of consolidation	Dissolution		Types of reservoir space
Stages	Periods	Ro (%)	Evolution model	Hydrocarbon evolution	Smectite in I/S (%)	I/S zone		Silicate minerals	Carbonate minerals	
Early	A	<0.35	Immature	Biogas	> 70	Smectite zone	Weak consolidation to semi consolidation			Mainly primary pores
	B	0.35-0.5			70-50	Disordered mixed layer zone				Semi consolidation to consolidation
Middle	A	0.5-1.3	Low mature -mature	Mainly oil	50-15	Ordered mixed layer zone	Consolidation			Primary pores are reserved and secondary pores are developed
	B	1.3-2.0	Highly mature	Condensed oil and wet gas	<15	Superlattice ordered mixed layer zone				Consolidation
Late		2.0-4.0	Postmature	Dry gas	Missing	Illite zone	Consolidation			Fractures are developed

FIGURE 15: Diagenetic evolution diagram showing the diagenetic stage of K<sub>2</sub>qn<sub>1</sub> in the SYY1 well, Qijia Sag, northern Songliao Basin (modified from the petroleum and natural gas industry standard of the People's Republic of China (SY/T 5477-2003)).



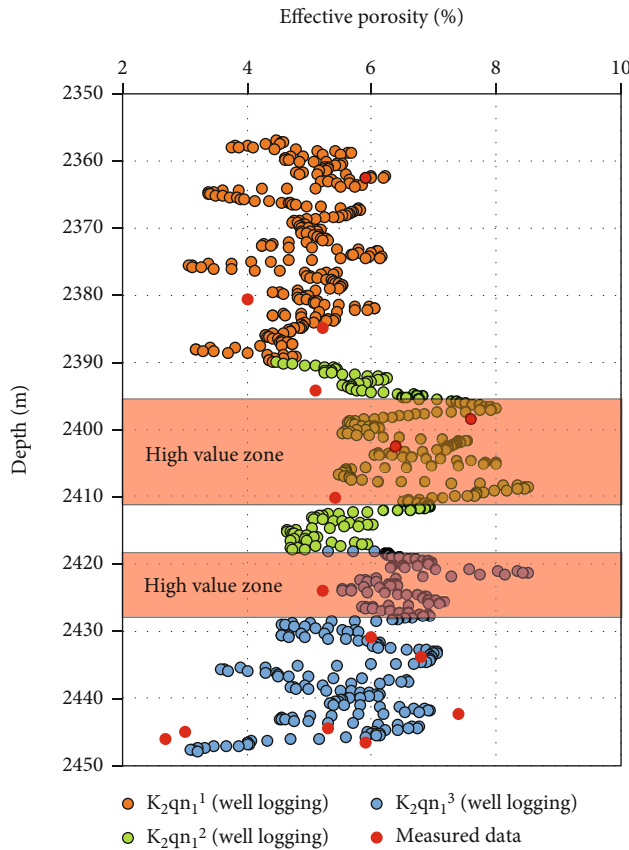


FIGURE 16: Graph of effective porosity with the depth of  $K_2qn_1$  core samples in the SYY1 well, Qijia Sag, northern Songliao Basin.

critical point ( $\sim 1.26\% R_0$ ) for the development of a large number of organic pores in the middle of the  $K_2qn_1^2$  submember (Table 2). Additionally, the organic matter in the lower part of  $K_2qn_1$  is more oil-prone with higher TOC (Figures 7 and 9), which may be more conducive to the formation of organic pores [46, 47]. Furthermore, organic acids produced during the hydrocarbon generation and organic matter evolution caused the dissolution of mineral particles and crystals, thus forming more intergranular dissolution pores in the lower part of  $K_2qn_1$ .

**4.4.2. Diagenetic Stages and Effective Porosity.** The average  $R_0$  of  $K_2qn_1$  in the SYY1 well is 1.26% (Table 2), which is at the late mature stage. The content of clay minerals is mainly illite, which ranges from 33% to 89% with an average of 66%, followed by chlorite and I/S (Table 3). The content of smectite in I/S is low between 15% and 25% with an average of 16% (Table 3). The reservoir space contains plenty of quartz, feldspar, and calcite dissolution pores as mentioned above (Figure 14). The above evidences indicate that  $K_2qn_1$  in the SYY1 well is in the late period of Middle Diagenesis A (Figure 15). The primary pores can be retained, and the release of organic acids leads to the increase in dissolution pores of mineral grains and meanwhile the formation of more organic pores during this stage.

As the effective porosity measurements are limited, we obtained more effective porosity data via interpreting the

high-resolution NMR logging in the SYY1 well calibrated by the measured data. The results show that the effective porosity of  $K_2qn_1^1$  is 3.06%-6.22% with an average of 4.88%; that of the  $K_2qn_1^2$  submember is 4.47%-6.26% with an average of 6.26%; that of the  $K_2qn_1^3$  submember is 3.10%-8.50% with an average of 5.86% (Figure 16). Obviously, the effective porosity of  $K_2qn_1^2$  and  $K_2qn_1^3$  is better than that of  $K_2qn_1^1$ . On the whole, there are two high-porosity value zones, distributed in the middle-lower part of the  $K_2qn_1^2$  submember and the upper part of the  $K_2qn_1^3$  submember, respectively (Figure 16), which exactly correspond to the high-value zones of organic matter abundance and oil content (Figure 17). Those indicate that these two high values of physical properties are related to the development of secondary dissolution pores and organic pores.

Relative to the TOC and  $S_1$  values (Figures 8(a), 8(b), and 8(c)), the effective porosity values obtained from well logging interpretation at the drilling horizontal section of the SYY1HF well fluctuated slightly, and the effective porosity values near target A are greater than those near target C (Figures 8(a) and 8(d)). However, this difference in effective porosity can be related to the previous vertical fracturing of the SYY1 well in  $K_2qn_1$  and  $K_2qn_{2+3}$ , which greatly improved the physical properties of  $K_2qn_1$  near the wellbore trajectory of the SYY1 well. That is to say, the present effective porosity cannot reflect the original porosity characteristics of  $K_2qn_1$  close to target A at the drilling horizontal section and also at the drilling inclined section, while the effective porosity of  $K_2qn_1$  close to target C is similar to the real value at the drilling horizontal section.

**4.5. Enrichment Regularity of Shale Oil.** Based on the above analysis, the enrichment of shale oil in  $K_2qn_1^2$  and  $K_2qn_1^3$  of the SYY1 well is significantly better than that in  $K_2qn_1^1$  (Figure 17). In terms of organic geochemical characteristics,  $K_2qn_1^2$  and  $K_2qn_1^3$  have the higher abundance, better types, and slightly higher maturity of organic matter than  $K_2qn_1^1$ , so the oil generation capacity of  $K_2qn_1^2$  and  $K_2qn_1^3$  is better than that of  $K_2qn_1^1$ , which develops a good material basis for shale oil enrichment in  $K_2qn_1^2$  and  $K_2qn_1^3$ . In terms of oil-bearing property,  $S_1$ , OSI, EOM, and oil saturation of  $K_2qn_1^2$  and  $K_2qn_1^3$  are generally higher than those of  $K_2qn_1^1$ , and additionally, saturated hydrocarbon content in EOM is relatively higher, which indicates that  $K_2qn_1^2$  and  $K_2qn_1^3$  not only have better oil content but also contain more movable oil. In terms of reservoir characteristics, dissolution pores in mineral grains and organic pores in  $K_2qn_1^2$  and  $K_2qn_1^3$  are more developed, and the effective porosity of  $K_2qn_1^2$  and  $K_2qn_1^3$  is also significantly bigger than that of  $K_2qn_1^1$ , which provides better occurrence spaces for the shale oil enrichment of  $K_2qn_1^2$  and  $K_2qn_1^3$ . It was found that the intervals with good organic geochemical properties also are good in oil content and reservoir characteristics (Figure 17), which indicates that the shale oil of deep to semideep lacustrine facies of  $K_2qn_1$  in the study area is formed mainly by in situ retention of residual oil.

Furtherly, it was found that the lower part of the  $K_2qn_1^2$  submember and the upper part of the  $K_2qn_1^3$  submember contain more proportion of mudstones with less nonshale

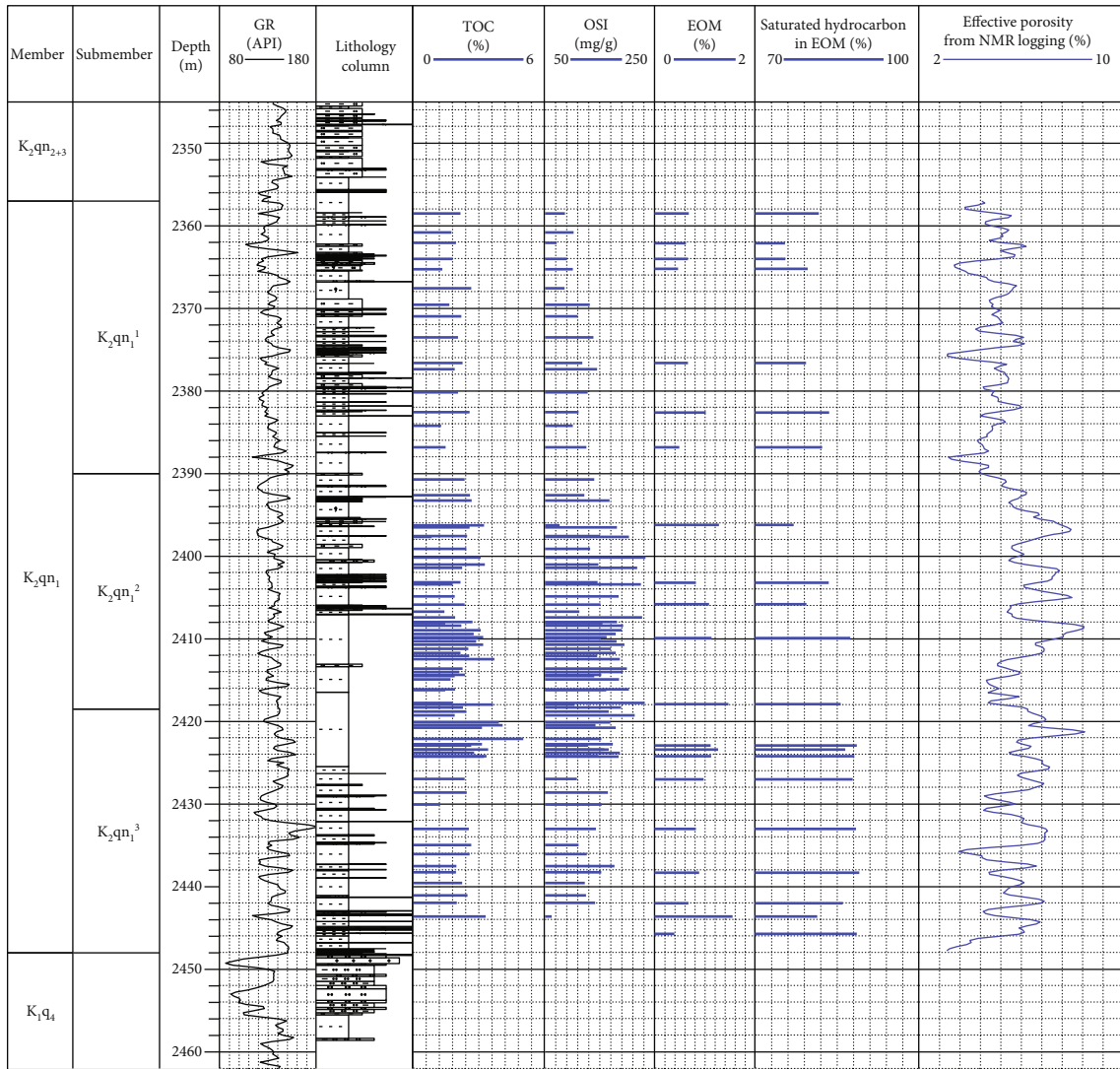


FIGURE 17: Comprehensive profile of typical geological and geochemical parameters of  $K_2qn_1$  in the SYY1 well, Qijia Sag, northern Songliao Basin.

interlayers, and their parameters relative to organic matter geochemical characteristics, oil-bearing property, and reservoir characteristics are generally better than those of the remaining part of  $K_2qn_1^2$  and  $K_2qn_1^3$  (Figure 17). Therefore, the lower part of the  $K_2qn_1^2$  submember and the upper part of the  $K_2qn_1^3$  submember are determined as the best intervals of shale oil enrichment for  $K_2qn_1$  vertically and should be the first target layer choice for shale oil exploration in the study area.

Based on the TOC,  $S_1$ , and effective porosity interpreted from the logging data of the SYY1HF well, it was found that there is a certain degree of horizontal heterogeneity in  $K_2qn_1$ . Compared with the effective porosity, the horizontal heterogeneity of TOC and  $S_1$  is stronger (Figure 8). Therefore, in the exploration of continental lacustrine matrix shale oil, it is necessary to predict the horizontal geological and geochemical parameters of the target layer accurately and to select the area with relatively weak heterogeneity for horizontal well drilling, so as to obtain a higher shale oil yield.

## 5. Conclusions

The lithology of  $K_2qn_1$  deposited in deep to semideep lacustrine facies of the Qijia Sag is mainly dark mudstone with few macrostructural fractures and belongs to the typical matrix reservoirs for shale oil. On the basis of lithology features and logging curves,  $K_2qn_1$  can be divided into three submembers including  $K_2qn_1^1$ ,  $K_2qn_1^2$ , and  $K_2qn_1^3$  from above to below.

On the whole, the conditions for shale oil enrichment in  $K_2qn_1$  are good in the Qijia Sag. Among the three submembers, shale oil in  $K_2qn_1^2$  and  $K_2qn_1^3$  is more enriched than that in  $K_2qn_1^1$  for the following reasons. First,  $K_2qn_1^2$  and  $K_2qn_1^3$  have better oil generation capacity with the higher abundance, better types, and slightly higher maturity of organic matter than  $K_2qn_1^1$ . Second,  $K_2qn_1^2$  and  $K_2qn_1^3$  are of higher oil content and more movable oil than  $K_2qn_1^1$ , which was supported by larger values in the parameters of  $S_1$ , OSI, EOM, oil saturation, and saturated hydrocarbon

content in EOM for  $K_2qn_1^2$  and  $K_2qn_1^3$ . Third,  $K_2qn_1^2$  and  $K_2qn_1^3$  with more intragranular dissolution pores and organic pores are of higher effective porosity than  $K_2qn_1^1$ .

By integrating all kinds of parameters including organic geochemical characteristics, oil-bearing property, and reservoir characteristics, the lower  $K_2qn_1^2$  and the upper  $K_2qn_1^3$  are regarded as the best intervals of shale oil enrichment in  $K_2qn_1$ . From the TOC,  $S_1$ , and effective porosity in the drilling horizontal section of the SYY1HF well, there is a certain horizontal heterogeneity in the  $K_2qn_1$  shale oil reservoir. Therefore, the lower  $K_2qn_1^2$  and the upper  $K_2qn_1^3$  in the area with relatively weak horizontal reservoir heterogeneity should be selected as the preferential targets for shale oil exploration in the Qijia Sag.

### Data Availability

The data used to support the findings of this study are included within the article.

### Conflicts of Interest

The authors declare that they have no conflicts of interest.

### Acknowledgments

The authors are grateful to Dr. Yan Liu in Yangtze University for the assistance with the analysis of kerogen macerals and sincerely thank Drs. Kaixi Jiang in Nanjing University, Zhaowen Zhan in Guangzhou Institute of Geochemistry, Chinese Academy of Sciences, and Jinqi Qiao in Germany's RWTH Aachen University for their constructive suggestions. This study was jointly supported by the Geological Survey Project of China Geological Survey (Grant Nos. DD20190114 and DD20190097); the Open Fund of State Key Laboratory of Organic Geochemistry, Guangzhou Institute of Geochemistry, Chinese Academy of Sciences (Grant No. SKLOG-201905); and the National Natural Science Foundation of China (Grant No. 42072178).

### References

- [1] J. C. Zhang, L. M. Lin, Y. X. Li et al., "Classification and evaluation of shale oil," *Earth Science Frontiers*, vol. 19, no. 5, pp. 322–331, 2012.
- [2] C. N. Zou, Z. Yang, J. W. Cui et al., "Formation mechanism, geological characteristics and development strategy of non-marine shale oil in China," *Petroleum Exploration and Development*, vol. 40, no. 1, pp. 14–26, 2013.
- [3] US Energy Information Administration (EIA), "Technically recoverable shale gas and shale oil resources: an assessment of 137 shale formations in 41 countries outside the United States," *EIA/ARI World Shale Gas and Shale Oil Resource Assessment*, pp. 6–7, 2013, <http://www.eia.gov/analysis/studies/worldshalegas/pdf/overview>.
- [4] C. N. Zou, S. Q. Pan, Z. H. Jing, J. L. G. Z. Yang, S. T. Wu, and Q. Zhao, "Shale oil and gas revolution and its impact," *Acta Petrolei Sinica*, vol. 41, no. 1, pp. 1–12, 2020.
- [5] D. Dong, Y. Wang, X. Li et al., "Breakthrough and prospect of shale gas exploration and development in China," *Natural Gas Industry B*, vol. 36, no. 1, pp. 19–32, 2016.
- [6] B. Liu, J. Shi, X. Fu et al., "Petrological characteristics and shale oil enrichment of lacustrine fine-grained sedimentary system: a case study of organic-rich shale in first member of Cretaceous Qingshankou Formation in Gulong Sag, Songliao Basin, NE China," *Petroleum Exploration and Development*, vol. 45, no. 5, pp. 1–11, 2018.
- [7] S. Chen, S. Zhang, Y. Wang, and M. Tan, "Lithofacies types and reservoirs of Paleogene fine-grained sedimentary rocks Dongying Sag, Bohai Bay Basin, China," *Petroleum Exploration and Development*, vol. 43, no. 2, pp. 218–229, 2016.
- [8] X. Z. Zhao, L. H. Zhou, M. Zhao, W. G. Wang, and Q. S. Guan, "Breakthrough and practice of industrial development on continental shale oil: a case study on Kong-2 member in Cangedong sag, Bohai Bay Basin," *China Petroleum Exploration*, vol. 24, no. 5, pp. 589–600, 2019.
- [9] H. Yang, X. Niu, L. Xu et al., "Exploration potential of shale oil in Chang7 member, Upper Triassic Yanchang Formation, Ordos Basin, NW China," *Petroleum Exploration and Development*, vol. 43, no. 4, pp. 511–520, 2016.
- [10] C. N. Zou, Z. Yang, S. S. Sun et al., "Exploring petroleum inside source kitchen: shale oil and gas in Sichuan Basin," *Science China Earth Sciences*, vol. 63, no. 7, pp. 934–953, 2016.
- [11] D. M. Zhi, Y. Tang, Z. F. Yang et al., "Geological characteristics and accumulation mechanism of continental shale oil in Jimusaer sag, Junggar Basin," *Oil & Gas Geology*, vol. 40, no. 3, pp. 524–534, 2019.
- [12] Z. L. Sun, F. R. Wang, Y. G. Hou et al., "Multi-scale characterization of the spatial distribution of movable hydrocarbon in intersalt shale of Qianjiang Formation, Qianjiang Sag, Jianghan Basin," *Petroleum Geology & Experiment*, vol. 42, no. 4, pp. 586–595, 2020.
- [13] B. Liu, Y. Lü, Y. Meng et al., "Petrologic characteristics and genetic model of lacustrine lamellar fine-grained rock and its significance for shale oil exploration: a case study of Permian Lucaogou Formation in Malang sag, Santanghu Basin, NW China," *Petroleum Exploration and Development*, vol. 42, no. 5, pp. 598–607, 2015.
- [14] M. W. Li, X. X. Ma, Q. G. Jiang, Z. M. Li, X. Q. Pang, and C. T. Zhang, "Enlightenment from formation conditions and enrichment characteristics of marine shale oil in North America," *Petroleum Geology and Recovery Efficiency*, vol. 26, no. 1, pp. 13–28, 2019.
- [15] M. W. Li, Z. J. Jin, M. Z. Dong et al., "Advances in the basic study of lacustrine shale evolution and shale oil accumulation," *Petroleum Geology & Experiment*, vol. 42, no. 4, pp. 489–505, 2020.
- [16] Z. P. Huo, S. B. Hao, B. Liu et al., "Geochemical characteristics and hydrocarbon expulsion of source rocks in the first member of the Qingshankou Formation in the Qijia-Gulong Sag, Songliao Basin, Northeast China: evaluation of shale oil resource potential," *Energy Science & Engineering*, no. 5, pp. 1–18, 2020.
- [17] B. Liu, J. H. Sun, Y. Q. Zhang et al., "Reservoir space and enrichment model of shale oil in the first member of Cretaceous Qingshankou Formation in the Changling sag, southern Songliao Basin, NE China," *Petroleum Exploration and Development*, vol. 48, no. 3, pp. 1–16, 2021.
- [18] S. C. Li, J. Y. Zhang, F. H. Gong, H. Zhu, and Y. F. Bai, "The characteristics of mudstones of Upper Cretaceous Qingshankou Formation and favorable area optimization of shale oil

- in the north of Songliao Basin,” *Geological Bulletin of China*, vol. 36, no. 4, pp. 654–663, 2017.
- [19] B. Liu, Y. F. Lü, Q. C. Ran, C. L. Dai, M. Li, and M. Wang, “Geological conditions and exploration potential of shale oil in Qingshankou Formation, northern Songliao Basin,” *Oil & Gas Geology*, vol. 35, no. 2, pp. 280–285, 2014.
- [20] K. X. Yang, J. Xiao, Y. Wang, and X. Ning, “A study on Qingshankou Formation’s tight oil characteristics and accumulation mode in the northern Songliao Basin,” *Acta Sedimentologica Sinica*, vol. 35, no. 3, pp. 600–610, 2017.
- [21] H. W. Zhang, *Study on Tight Oil Accumulation Conditions in Qijia Area of Songliao Basin*, Northeast Petroleum University, Daqing, Heilongjiang, China, 2017.
- [22] J. Y. Zhang, “Main controlling factors of oiliness property of tight sandstone reservoir within source rock in continental depression basin: a case of Gaotaizi oil reservoir in Qijia sag of central depression area in northern Songliao Basin,” *Acta Sedimentologica Sinica*, vol. 34, no. 5, pp. 991–1002, 2016.
- [23] J. G. Yang, S. C. Li, Y. L. Yao et al., “Significant breakthrough in the continental shale oil survey in northern Songliao Basin,” *Geology and Resources*, vol. 29, no. 3, p. 300, 2020.
- [24] H. Xue, S. Tian, S. Lu, W. H. Zhang, and G. D. Mu, “Selection and verification of key parameters in the quantitative evaluation of shale oil: a case study at the Qingshankou Formation, northern Songliao Basin,” *Bulletin of Mineralogy, Petrology and Geochemistry*, vol. 34, no. 1, pp. 70–78, 2015.
- [25] Y. H. Wu, T. F. Lin, Y. F. Bai et al., “Analyses of the mudstone (shale) oil exploration potential in north Songliao Basin,” *Petroleum Geology & Oilfield Development in Daqing*, vol. 38, no. 5, pp. 78–86, 2019.
- [26] F. Chen, S. Lu, Z. Huang, W. Wang, Z. Xie, and H. Xiao, “Sedimentary characteristics and favorable exploration zone of K<sub>1</sub>qn<sup>1</sup> in Gulong depression of Songliao Basin,” *Journal of Central South University (Science and Technology)*, vol. 44, no. 5, pp. 1955–1963, 2013.
- [27] Y. Zhao and J. Y. Zhang, “Geological conditions and exploration potential for shale oil of Qingshankou Formation in Gulong sag,” *Geological Review*, vol. 66, no. supp. 1, pp. 119–120, 2020.
- [28] B. W. Cui, C. R. Chen, X. D. Lin et al., “Characteristics and distribution of sweet spots in Gulong shale oil reservoirs of Songliao Basin,” *Petroleum Geology & Oilfield Development in Daqing*, vol. 39, no. 3, pp. 45–55, 2020.
- [29] M. C. Jia, *Reservoir Characteristics and Oil Enrichment Rule of Shale Series in the First Member of Qingshankou Formation in Gulong Sag*, Northeast Petroleum University, Daqing, Heilongjiang, China, 2017.
- [30] J. Lu, *Fine Sedimentary Cycles and Heterogeneity of Qingshankou Formation in Gulong Sag*, Northeast Petroleum University, Daqing, Heilongjiang, China, 2017.
- [31] Z. Liu, J. Song, X. Liu, X. Wu, and X. Gao, “Discovery of the Cretaceous-Paleogene compressional structure and basin properties of the southern Songliao Basin,” *Acta Petrologica Sinica*, vol. 36, no. 8, pp. 2383–2393, 2020.
- [32] B. Liu, S. He, L. Meng, X. Fu, L. Gong, and H. Wang, “Sealing mechanisms in volcanic faulted reservoirs in Xujiaweizi extension, Northern Songliao Basin, Northeastern China,” *AAPG Bulletin*, vol. 105, no. 8, 2021.
- [33] P. J. Wang, F. Mattern, N. A. Didenko, D. F. Zhu, B. Singer, and X. M. Sun, “Tectonics and cycle system of the Cretaceous Songliao Basin: an inverted active continental margin basin,” *Earth-Science Reviews*, vol. 159, pp. 82–102, 2016.
- [34] P. Allix, A. Burnham, T. Fowler, M. Herron, R. Kleinberg, and B. Symington, “Coaxing oil from shale,” *Oilfield Review Winter*, vol. 22, no. 4, p. 5, 2011.
- [35] B. P. Tissot and D. H. Welte, *Petroleum Formation and Occurrence*, Springer-Verlag, Berlin, 2nd edition, 1984.
- [36] D. F. Huang, J. C. Li, Z. H. Zhou, X. Z. Gu, and D. J. Zhang, *Evolution and Hydrocarbon Generation Mechanism of Terrestrial Organic Matter*, Petroleum Industry Press, Beijing, 1984.
- [37] S. F. Lu and M. Zhang, *Petroleum Geochemistry*, Petroleum Industry Press, Beijing, 2008.
- [38] D. Song, X. Wang, C. Wu et al., “Petroleum generation, retention, and expulsion in lacustrine shales using an artificial thermal maturation approach: implications for the in-situ conversion of shale oil,” *Energy & Fuels*, vol. 35, no. 1, pp. 358–373, 2021.
- [39] K. E. Peters and M. R. Casa, “Applied source rock geochemistry,” in *The Petroleum System: From Source to Trap*, L. B. Magoon and W. G. Dow, Eds., pp. 93–120, American Association of Petroleum Geologists, Tulsa, 1994.
- [40] L. Luo, D. Tan, X. Zha et al., “Enrichment factors and resource potential evaluation of Qingshankou Formation lacustrine shale oil in the Southern Songliao Basin, NE China,” *Geofluids*, vol. 2021, Article ID 6645467, 20 pages, 2021.
- [41] J. Q. Qiao, A. Baniasad, L. Zieger, C. Zhang, Q. Luo, and R. Littke, “Paleo-depositional environment, origin and characteristics of organic matter of the Triassic Chang 7 member of the Yanchang Formation throughout the mid-western part of the Ordos Basin, China,” *International Journal of Coal Geology*, vol. 237, article 103636, 2021.
- [42] D. M. Jarvie, “Shale resource systems for oil and gas: part 2 – shale-oil resource systems,” in *Shale Reservoirs – Giant Resources for the 21st century*, J. A. Breyer, Ed., vol. 97, pp. 89–119, AAPG Memoir, 2012.
- [43] H. T. Xue, S. S. Tian, W. M. Wang, W. H. Zhang, T. T. Du, and G. D. Mu, “Correction of oil content—one key parameter in shale oil resource assessment,” *Oil & Gas Geology*, vol. 37, no. 1, pp. 15–22, 2016.
- [44] K. L. Milliken, W. L. Esch, R. M. Reed, and T. Zhang, “Grain assemblages and strong diagenetic overprinting in siliceous mudrocks, Barnett Shale (Mississippian), Fort Worth Basin, Texas,” *AAPG Bulletin*, vol. 96, no. 8, pp. 1553–1578, 2012.
- [45] M. E. Curtis, B. J. Cardott, C. H. Sondergeld, and C. S. Rai, “Development of organic porosity in the Woodford Shale with increasing thermal maturity,” *International Journal of Coal Geology*, vol. 103, pp. 26–31, 2012.
- [46] C. Yang, Y. Q. Xiong, and J. C. Zhang, “Developmental differences of secondary organic pores among marine, lacustrine, and transitional shale in China,” *Geochimica*, vol. 48, no. 6, pp. 544–554, 2019.
- [47] B. Liu, Y. Gao, K. Liu et al., “Pore structure and adsorption hysteresis of the middle Jurassic Xishanyao shale formation in the Southern Junggar Basin, northwest China,” *Energy Exploration & Exploitation*, pp. 1–18, 2021.